

AD-A038 298

ARCON CORP WAKEFIELD MASS
IONOSPHERIC ANALYSIS AND IONOSPHERIC MODELING.(U)
FEB 77 D C MILLER, J GIBBS

F/G 20/14

UNCLASSIFIED

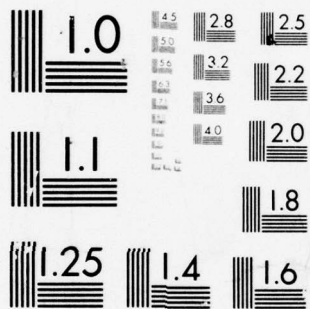
RADC-TR-77-53

F19628-74-C-0070

NL

1 OF 2
AD
A038 298





MICROCOPY RESOLUTION TEST CHART
NATIONAL BUREAU OF STANDARDS-1963-A

RADC-TR-77-53
Final Technical Report

(2)

AD A 038298

IONOSPHERIC ANALYSIS AND
IONOSPHERIC MODELING

ARCON Corporation
Lakeside Office Park
Wakefield, Massachusetts 01880

Approved for Public Release;
Distribution Unlimited

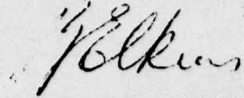
ROME AIR DEVELOPMENT CENTER
Air Force Systems Command
Griffiss Air Force Base, New York 13441

AD No. _____
DDC FILE COPY

BR

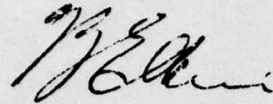
This report has been reviewed by the RADC Information Office (OI) and is releasable to the National Technical Information Service (NTIS). At NTIS it will be releasable to the general public, including foreign nations.

APPROVED:



TERENCE J. ELKINS
Contract Monitor
Electromagnetic Sciences Division

APPROVED:

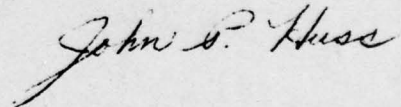


TERENCE J. ELKINS, Chief
Ionospheric Radio Physics Branch
Electromagnetic Sciences Division

APPROVED:



ALLAN C. SCHELL, Acting Chief
Electromagnetic Sciences Division



Do not return this copy. Retain or destroy.

Unclassified

SECURITY CLASSIFICATION OF THIS PAGE (When Data Entered)

19 REPORT DOCUMENTATION PAGE		READ INSTRUCTIONS BEFORE COMPLETING FORM
1. REPORT NUMBER RADC-TR-77-53	2. GOVT ACCESSION NO.	3. RECIPIENT'S CATALOG NUMBER
4. TITLE (and Subtitle) IONOSPHERIC ANALYSIS AND IONOSPHERIC MODELING		5. TYPE OF REPORT & PERIOD COVERED Final rept. July 1973 - Oct 1976
7. AUTHOR(s) David C. Miller Joseph Gibbs		6. PERFORMING ORG. REPORT NUMBER
9. PERFORMING ORGANIZATION NAME AND ADDRESS ARCON Corporation 18 Lakeside Office Park Wakefield, Massachusetts 01880		8. CONTRACT OR GRANT NUMBER(s) F19628-74-C-0070
11. CONTROLLING OFFICE NAME AND ADDRESS Deputy for Electronic Technology (RADC/ETEI) Hanscom AFB, Massachusetts 01731 Contract Monitor: Samuel Horowitz		10. PROGRAM ELEMENT, PROJECT, TASK AREA & WORK UNIT NUMBERS 5631-18-01 61102F
14. MONITORING AGENCY NAME & ADDRESS (if different from Controlling Office) 1299p.		12. REPORT DATE February 1977
		13. NUMBER OF PAGES 98
		15. SECURITY CLASS. (of this report) Unclassified
		15a. DECLASSIFICATION/DOWNGRADING SCHEDULE
16. DISTRIBUTION STATEMENT (of this Report) Approved for public release; distribution unlimited.		
17. DISTRIBUTION STATEMENT (of the abstract entered in Block 20, if different from Report)		
18. SUPPLEMENTARY NOTES Tech Other		
19. KEY WORDS (Continue on reverse side if necessary and identify by block number) Ionospheric Modeling Quasi Parabolic Ionosphere Polar Ionospheric Ionospheric Ray Tracing Electron Density Profiles		
20. ABSTRACT (Continue on reverse side if necessary and identify by block number) This report describes several investigations performed towards improving our ability to communicate through the ionospheric medium. These studies covered two distinct and separate areas. The first was concerned with improvements in ionospheric forecasting in the polar region through the development of empirical models for electron density profiles and ionospheric parameters. The second consisted of the study of various techniques for the establishment of high frequency communication circuit		

DD FORM 1 JAN 73 1473 EDITION OF 1 NOV 65 IS OBSOLETE

Unclassified

SECURITY CLASSIFICATION OF THIS PAGE (When Data Entered)

403 370

next
page

mt

Unclassified

SECURITY CLASSIFICATION OF THIS PAGE(When Data Entered)

cont

parameters. Attempts have been made to accurately determine ray paths for ionospheres with simple gradients without the use of three dimensional ray tracing techniques.



Unclassified

SECURITY CLASSIFICATION OF THIS PAGE(When Data Entered)

EVALUATION

F19628-74-C-0070 - ARCON Corporation

1. The final report on "Ionospheric Analysis and Ionospheric Modelling", Contract No. F19628-74-C-0070 consists of four sections. In the modelling effort of foF2, daily hourly observations of six years of the 1958/68 time span have been incorporated for adjusting the ITS model to the polar region. No significant improvement over the ITS model is claimed to have been noted after testing. In ray-tracing studies for parabolic and quasi-parabolic electron-density height variations and horizontal gradients a transmitter-coordinate-system was introduced to facilitate the assessment of the effects of longitudinal and transverse gradients on propagation characteristics. An iterative scheme was developed to place a nominal electron density profile near ray reflection. A functional representation of effective tilt in a parabolic ionosphere was deduced. The three-dimensional-model effort dealt with the synthesis of electron density height profiles by means of a three-layer ionosphere considering monotonically increasing electron density profiles as well as those possessing an ionization valley. Procedures for proper matching of profile segments of contiguous layers were developed. The coordinate conversion technique for OTH backscatter radar applications, which is to appear in a separate report, is summarized. A given ionosphere is used to generate the leading edge of a backscatter ionogram. The latter is compared with a given backscatter ionogram. Range-gradient adjustment factors are applied to achieve mutual agreement. Once agreement is reached, predicted radio frequency paths are simulated and used to establish the relationship between ground range and group path. Eventually, this relationship is expected to yield estimates of ground range for an OTH-radar target.

2. The above work is of value since it provides computational procedures for utilizing and correcting for ionospheric radio propagation effects. These procedures will be used by USAF for further refinement of the ionosphere model to more realistically predict long-range ducting in ionospheric channels and to better estimate ground range to targets.

Terence J. Elkins

TERENCE J. ELKINS
Contract Monitor
Ionospheric Radio Physics Branch
Electromagnetic Sciences Division

RECEIVED BY	
RTS	White Section <input checked="" type="checkbox"/>
ROC	Ref Section <input type="checkbox"/>
UNANNOUNCED	
JUSTIFICATION	
BY	
EXTENSION OF EVALUATION CODES	
DATE	APPROVAL SPECIAL
A	

TABLE OF CONTENTS

<u>Section</u>		<u>Page</u>
I.	MODELING f_oF_2 IN THE POLAR REGION.	4
II.	STUDIES OF IONOSPHERIC RAY TRACING IN PARABOLIC IONOSPHERES WITH GRADIENTS.	32
III.	VERTICAL-ELECTRON-DENSITY MODELS IN THE POLAR REGION.	77
IV.	COORDINATE CONVERSION TECHNIQUE FOR OTH BACKSCATTER RADAR.	94

I. MODELING foF2 IN THE POLAR REGION

In this section, we will present some of our results from a study to improve our knowledge of the F2 region of the ionosphere in the polar region using an empirical model. In a previous report⁽¹⁾, we described some attempts at finding more accurate models of foF2. The motivation and method of approach to modeling foF2 remain the same as in our earlier work.

The ITS monthly median model⁽²⁾ for foF2 has been shown to represent the physical behavior of the ionosphere quite well in the midlatitude regions of the globe. We have, therefore, chosen to use this model as a first approximation for the determination of foF2 at high latitudes. Corrections to the model are then applied as functions of the relevant spatial and geophysical variables. While the ITS model is only based on median vertical incidence ionosonde data for IGY1958, we have used daily-hourly observations for 1958, 1960, 1962, 1964, 1966 and 1968 in the determination of correction terms for the polar region. The use of the daily data allowed for the inclusion of the planetary magnetic activity index, K_p dependence of foF2 in the model. Our earlier modeling of foF2 was based primarily on the 1958 and 1964 data and the resulting changes in the model reflect in large part the use of available data from other years.

The ITS monthly median model represents the median behavior of foF2 in terms of a spherical harmonic expansion of the space and time variables. The representation is of the form

$$\text{foF2} = \sum_{k=0}^N D_k(T) G_k(\theta, \lambda) \text{ where } \theta \text{ and}$$

λ are the geographic longitude and latitude and T is the universal time. Here the diurnal variation has been separated from the spatial variation and the cutoff parameter of the series, N is equal to 75. The time dependent functions are expanded in a Fourier series containing six harmonics:

$$D_k(T) = A_0^{(k)} + \sum_{j=1}^6 (A_j^{(k)} \cos jT + B_j^{(k)} \sin jT).$$

This results in a function

$$\begin{aligned} \text{foF2} = & \sum_{k=0}^N A_0^{(k)} G_k(\emptyset, \lambda) + \\ & \sum_{k=0}^N \sum_{j=1}^6 [A_j^{(k)} \cos(jT) G_k(\emptyset, \lambda) + B_j^{(k)} \sin(jT) G_k(\emptyset, \lambda)] \end{aligned}$$

where the $G(\emptyset, \lambda)$ are linear combinations of surface spherical harmonics. The explicit arguments of the G functions were chosen to be the modified magnetic dip angle x , λ and \emptyset . The modified magnetic dip angle is a function of the latitude and magnetic dip angle I , given by

$$I = \tan^{-1} \left[\frac{-B_z}{\sqrt{B_x^2 + B_y^2}} \right] \quad \text{where}$$

B_x , B_y , B_z are the north, east and vertical components of the earth magnetic field vector. The modified magnetic dip angle, x , is then

$$x = \tan^{-1} \left\{ \frac{I}{\sqrt{\cos \lambda}} \right\}$$

The 988 coefficients were determined using the hourly observations of foF2 that were available from a network of vertical-incidence ionosondes for the IGY 1958. The use of additional data from 1964 allowed for the determination of the mean sunspot number dependence of the coefficients.

The stations in the polar region for which foF2 data was available for the even years between 1960 and 1968 are listed in Table I-1. Approximately 100,000 hourly observations of foF2 were available for each of the years. While the stations do not give uniform coverage over the polar region, they can be used to explore some of the spatial and temporal features of the F2 region if one does not use them directly with simple regression techniques.

We have assumed that some of the corrections which are necessary for the polar region are strongly coupled to solar phenomena and, therefore, separate all observations into the two categories of solar day where χ (solar zenith angle) $\leq 94.6^\circ$ and solar night, $\chi > 94.6^\circ$. In addition to the foF2, we have made use of a data base of values of the three-hour planetary-magnetic-activity index, K_p for all of the years under study.

The polar ionosphere can be described in terms of dynamic effect which occur relative to several spatial boundaries. The most notable ones being the trough and auroral oval. In our previous work, we assumed that

TABLE I-1

Stations for Which foF2 Data is Available for 1960, 1962, 1964, 1966, 1968

<u>Stations</u>		<u>λ (Degrees)</u>	<u>λ_m (Degrees)</u>	<u>Φ (Degrees)</u>
Gorky	156	56.2	51.6	44.3
Julensruk	055	54.6	62.5	13.4
Kiruna	167	67.8	64.3	20.5
Leningrad	160	60.0	55.8	30.3
Lindau	050	51.4	48.3	10.1
Lycksele	164	64.6	61.2	18.8
Miedzeszyn	152	52.2	48.2	21.2
Moscow	155	55.5	51.0	37.3
Murmansk	168	68.9	64.6	33.0
Nurmijarvi	159	60.5	56.6	24.6
Providenya	664	64.4	60.3	18.5
Sakekhard	266	66.6	61.8	66.6
Slough	051	51.5	49.9	359.4
Sodankyla	166	67.4	63.4	26.6
Uppsala	158	59.8	56.4	17.6
Yakutsk	462	62.0	56.4	129.8

the boundaries were well established from earlier studies and examined the observations relative to these specified boundaries. It was apparent from our data that the spatial position and magnitude of any polar region corrections to foF2 were strongly correlated and varied widely from one year to another. For this reason, we have used each set of station-month data to determine all the properties of any feature of the ionosphere if it exists in the data. In addition to the geographic coordinates, universal time, and sunspot number used by the ITS model we have searched for corrections which may also be functions of the corrected geomagnetic space and time coordinates and the K_p index. As a first attempt to assess the accuracy of the median model, we have used each of the six years foF2 data to calculate the RMS residual Δ_{RMS} given by:

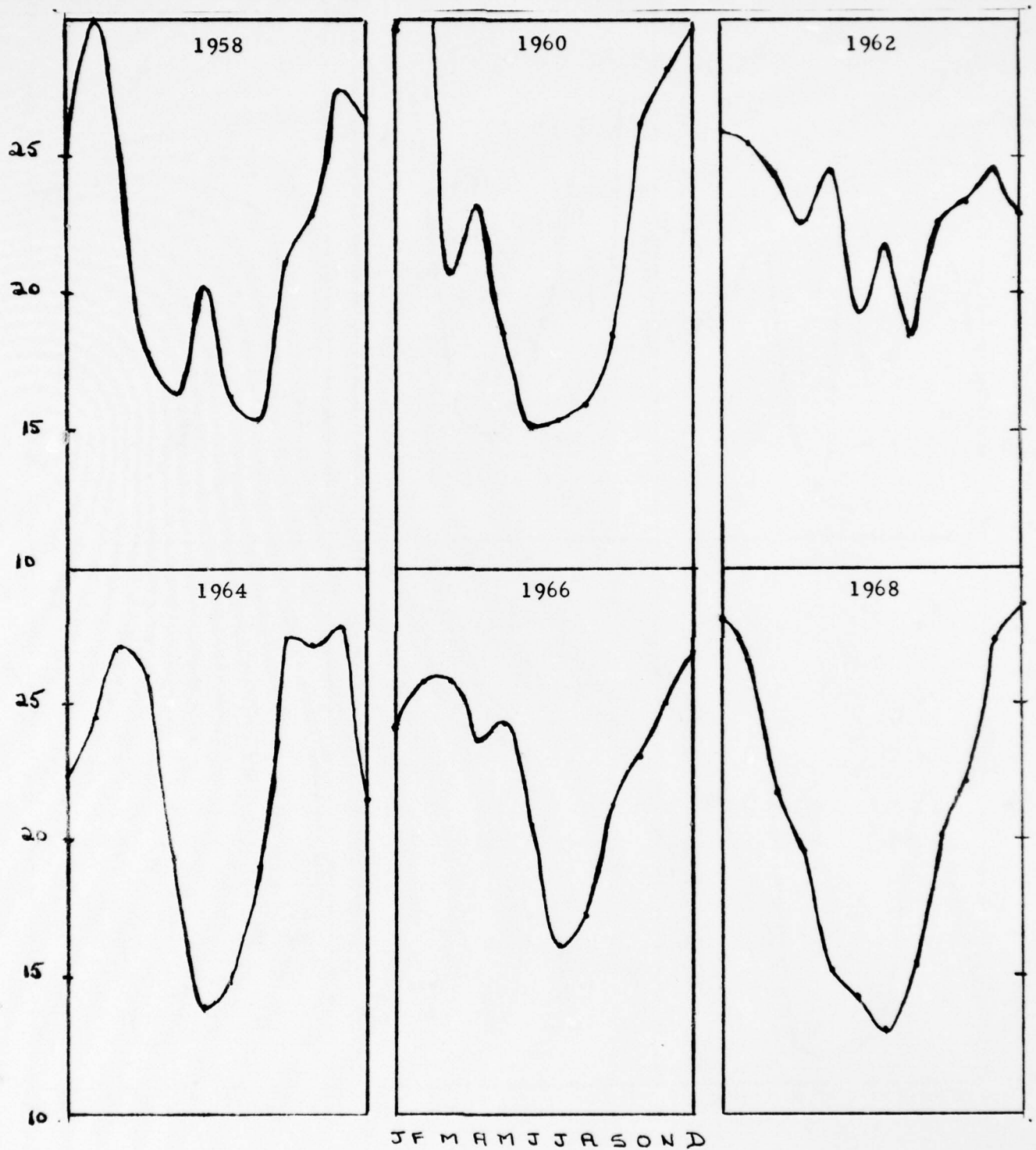
$$\Delta_{RMS}^2 = \frac{1}{N} \sum_{i=1}^N \left(\frac{foF2_i^{ITS} - foF2_i^{obs}}{foF2_i^{ITS}} \right)^2$$

where the index i denotes an individual measurement for a specific universal time, θ , λ , sunspot number and K_p . We first calculate Δ_{RMS} for each month and for solar day and night separately averaging over all station positions, time and daily geophysical parameters. The results are shown in the twelve curves of Figures I-1 and I-2.

Although the median model does contain a dependence on solar activity, the data presented in this form does indicate both random variations and systematic deficiencies of the model. The solar day data 1966 appears to give a good indication of the minimum random RMS error of the model of

SOLAR NIGHT

Percentage RMS Residuals with ITS Median Model, Δ_{RMS}

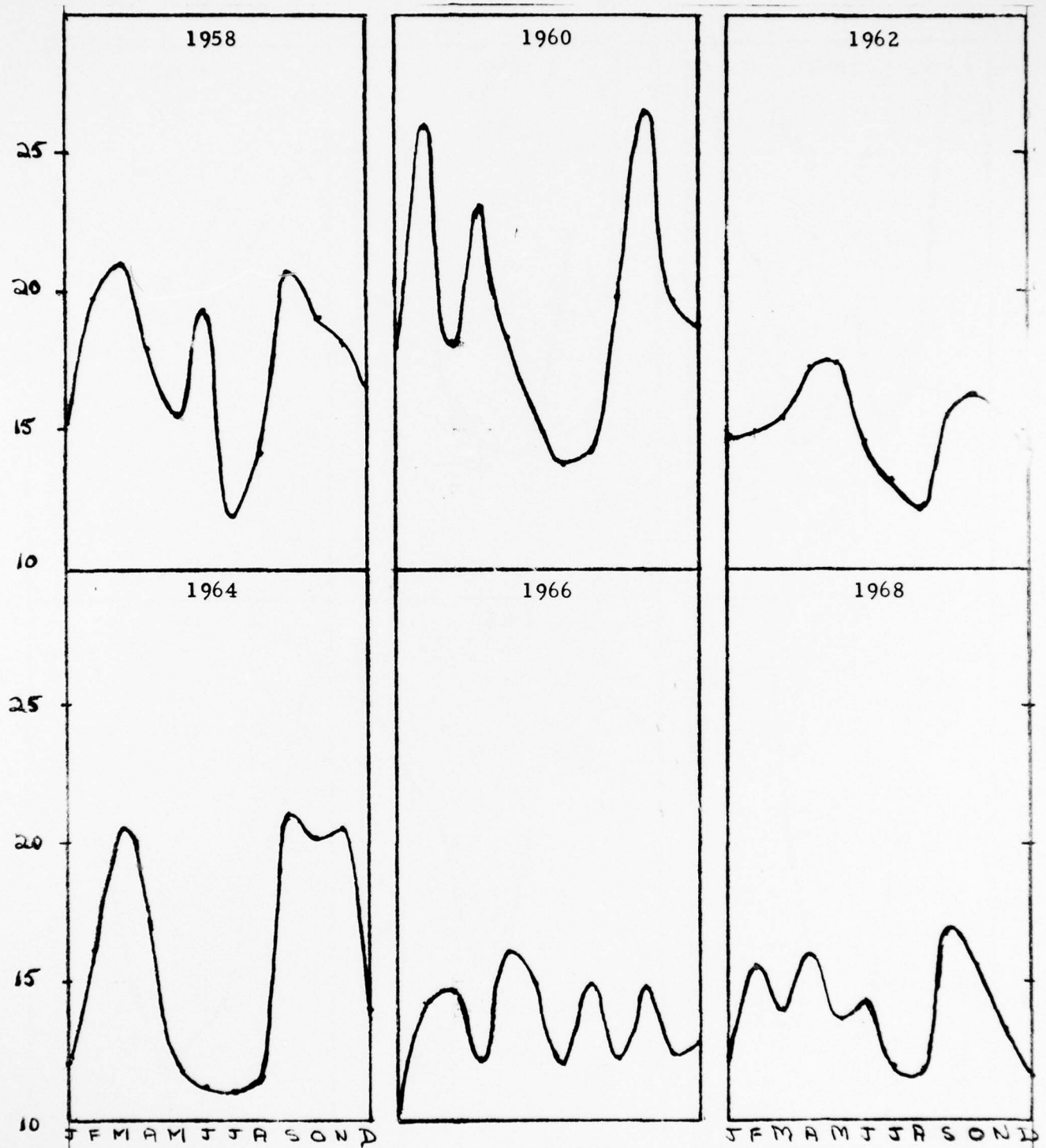


Month

Figure I-1

SOLAR DAY

Percentage RMS Residuals with ITS Median Model, Δ_{RMS}

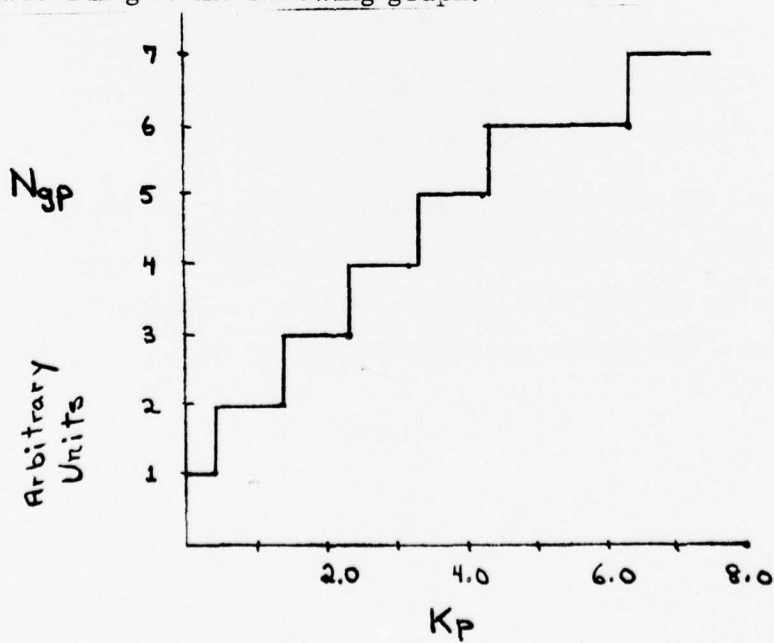


Month

Figure I-2

approximately 15%. This also appears to be of the same order in 1962 and 1968, but there is some evidence of systematic effects occurring during the spring and fall equinox. This effect is much more pronounced during the other three years. The difference between the solar night (SN) and solar day (SD) data varies greatly over the years. In 1964, the SN residual is almost a constant scale factor times the SD residual for each month of the year while the SN residuals of 1968 exhibit a strong seasonal dependence when none was present in the SD residuals. This strong seasonal nighttime effect is present in all the years with the ratio $\Delta_{\text{RMS}}(\text{winter}) / \Delta_{\text{RMS}}(\text{summer})$ being a factor of 2 for five of the six years. It should be emphasized that although these residuals are only determined for the set of polar region stations, the coverage of the region may still be biased with respect to individual dynamic features of the F2 region of the ionosphere.

In order to determine the corrections to the ITS model for foF2, we have divided the data into intervals of values of the magnetic activity index and the corrected geomagnetic latitude. Reasonable statistics were obtained by using 4° intervals of geomagnetic latitude beginning at 46° North. The 1958 data extended to 74° N while all the other years only gave adequate coverage to 62° N. The data was divided into seven intervals of magnetic activity according to the following graph.



For convenience, we present the data in only three categories of magnetic activity:

Low	$K_p \leq 1.3$
Medium	$1.3 < K_p \leq 3.3$
High	$3.3 < K_p$

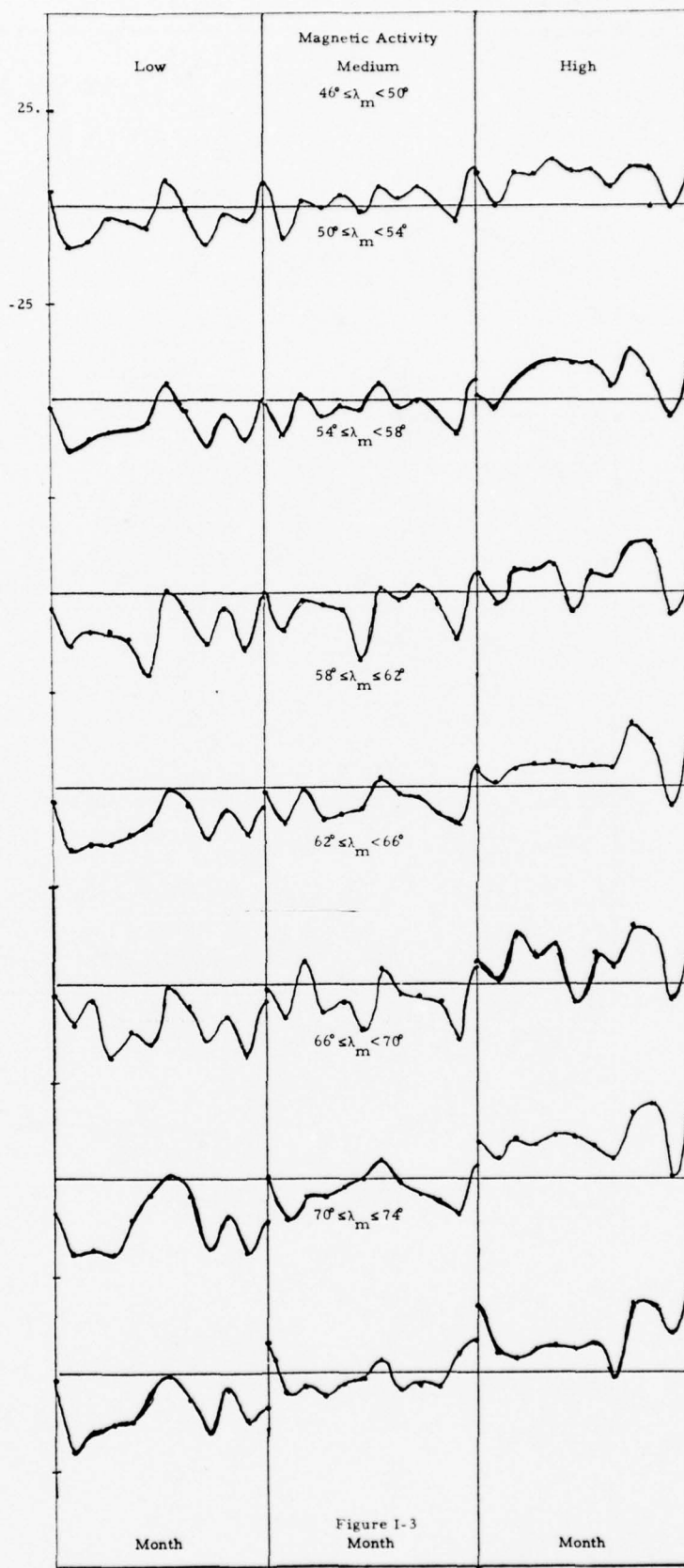
For each grouping of geomagnetic latitude and magnetic activity, we calculate the average percent residual:

$$\Delta(\lambda_m, K_p) = \frac{1}{N} \sum_{i=1}^N \left(\frac{foF2_i^{ITS} - foF2_i^{obs}}{foF2_i^{ITS}} \right)$$

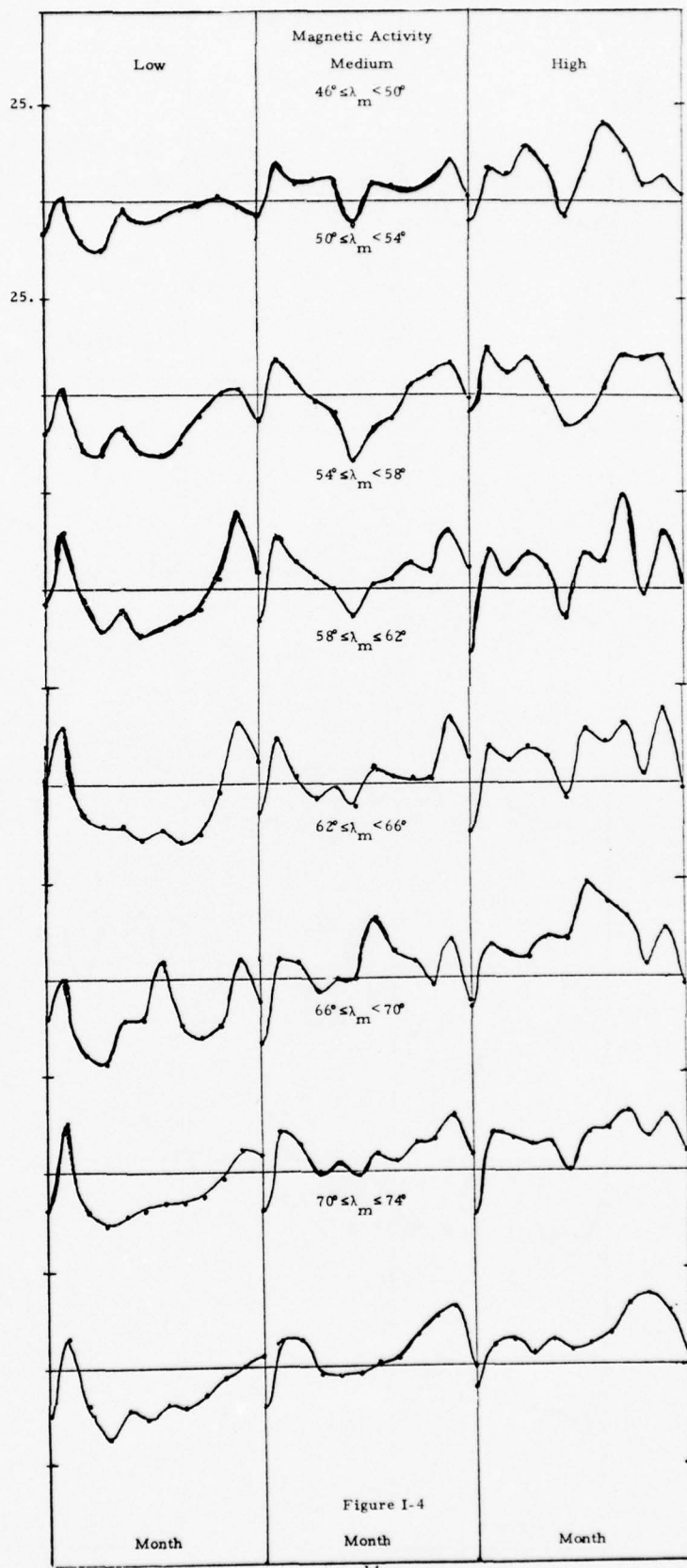
where the summation is performed for all stations and time. The results are presented as a function of the month number in Figures I-3 through I-14 for each of the years in the study. A strong feature of almost all the data is the similar K_p dependence of the average residual for each separate latitudinal interval. The correction is negative for low magnetic activity and positive for high magnetic activity. If the three groups are averaged, the results are consistent with the median model which was formulated without any dependence on magnetic activity.

The solar day and night residuals for 1958 do not exhibit any noticeable dependence upon geomagnetic latitude. There is also very little difference between the day and nighttime curves. This is consistent with earlier work in which very little evidence for the trough and auroral oval was observed

AVERAGE PERCENT RESIDUAL: SOLAR DAY 1958



AVERAGE PERCENT RESIDUAL: SOLAR NIGHT 1958



AVERAGE PERCENT RESIDUAL: SOLAR DAY 1960

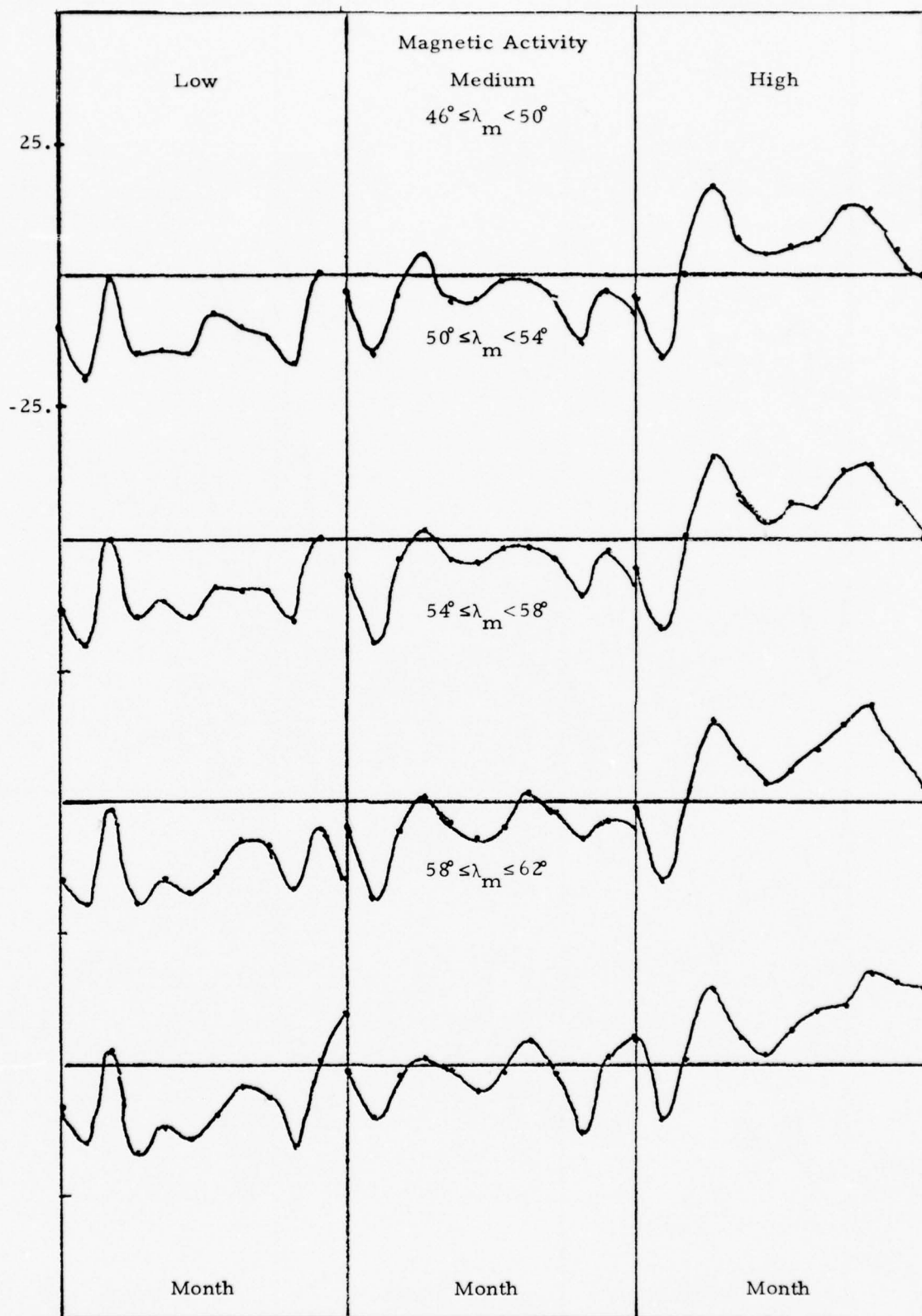


Figure I-5
15

AVERAGE PERCENT RESIDUAL: SOLAR NIGHT 1960

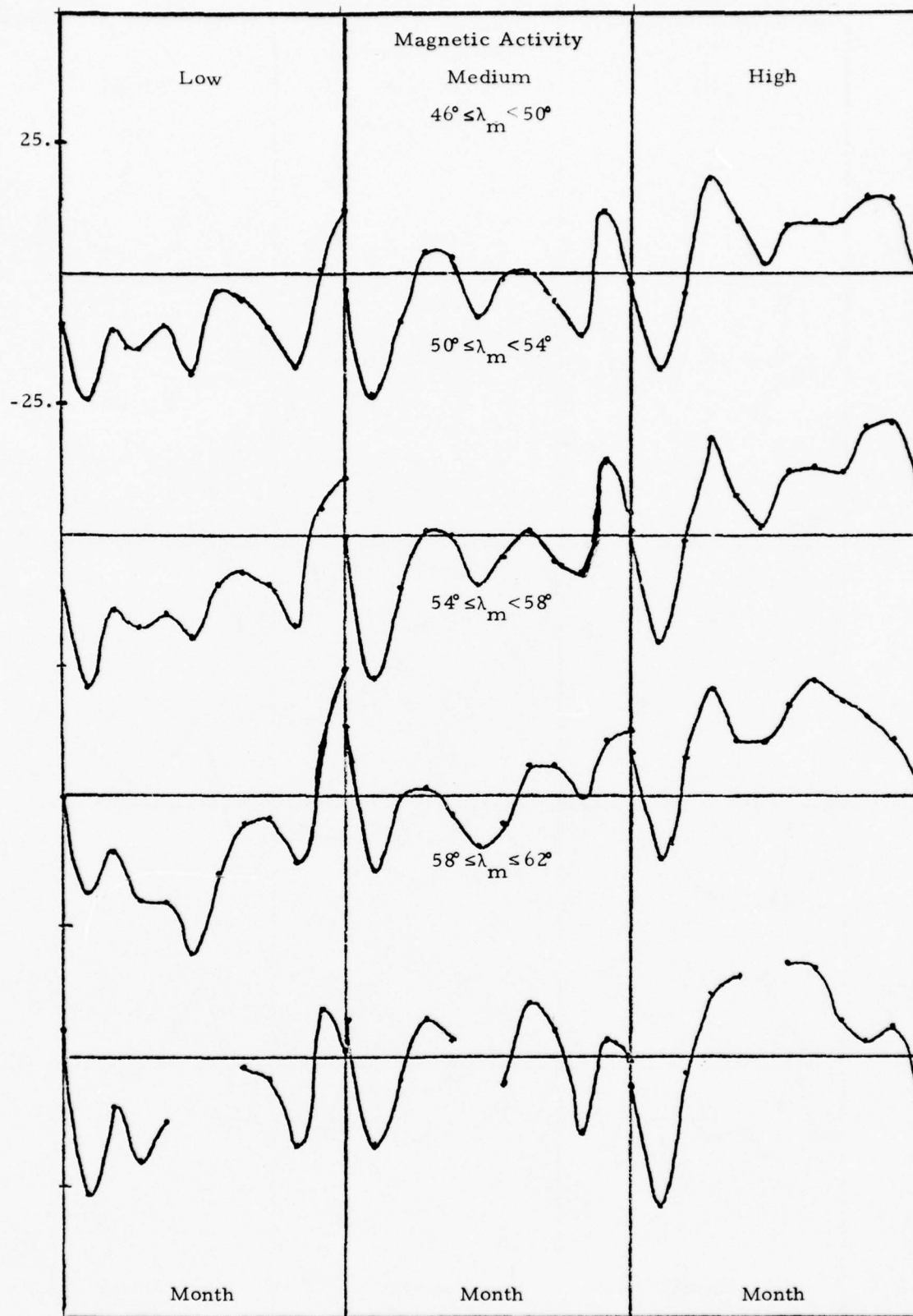


Figure I-6
16

AVERAGE PERCENT RESIDUAL: SOLAR DAY 1962

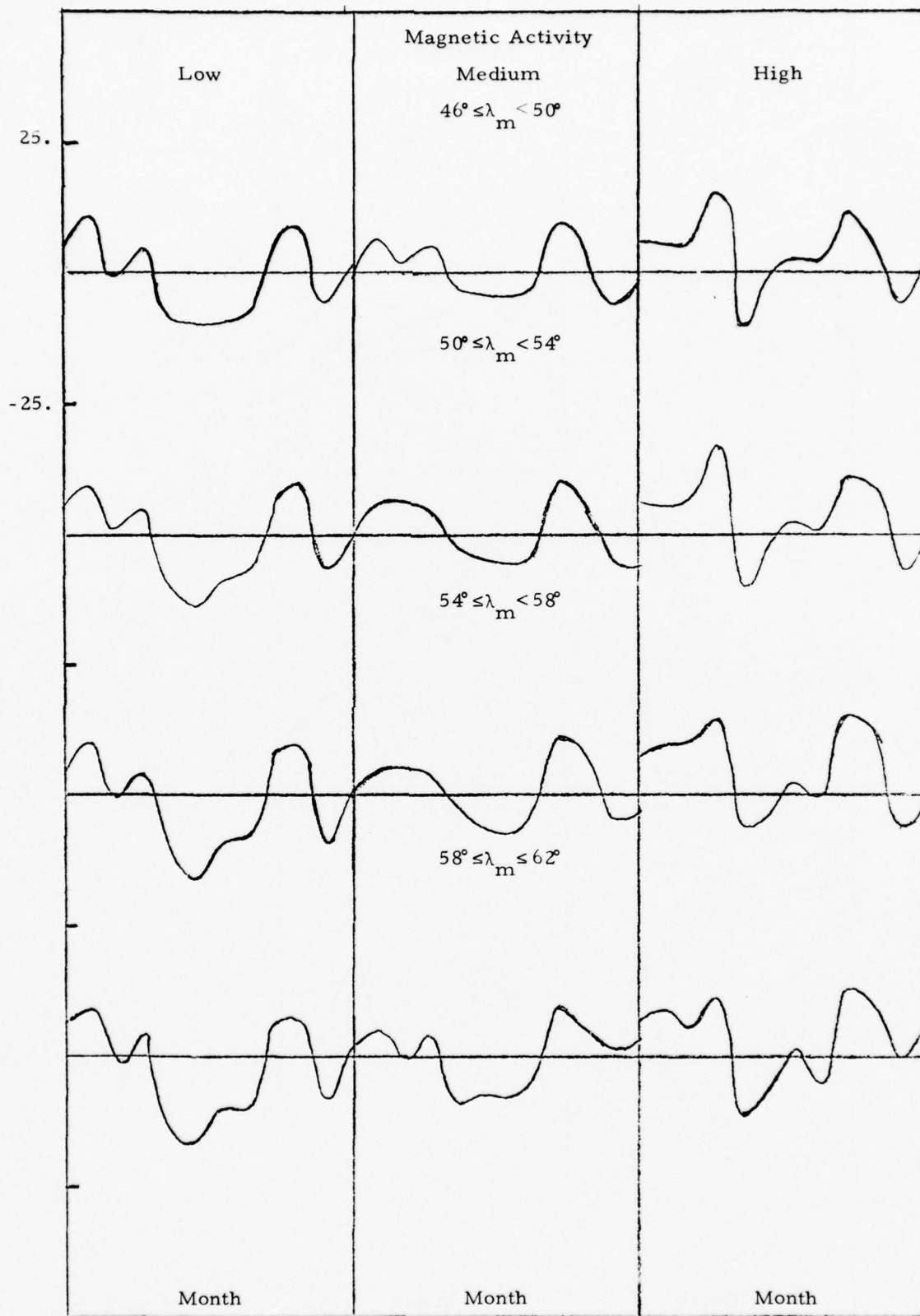


Figure I-7
17

AVERAGE PERCENT RESIDUAL: SOLAR NIGHT 1962

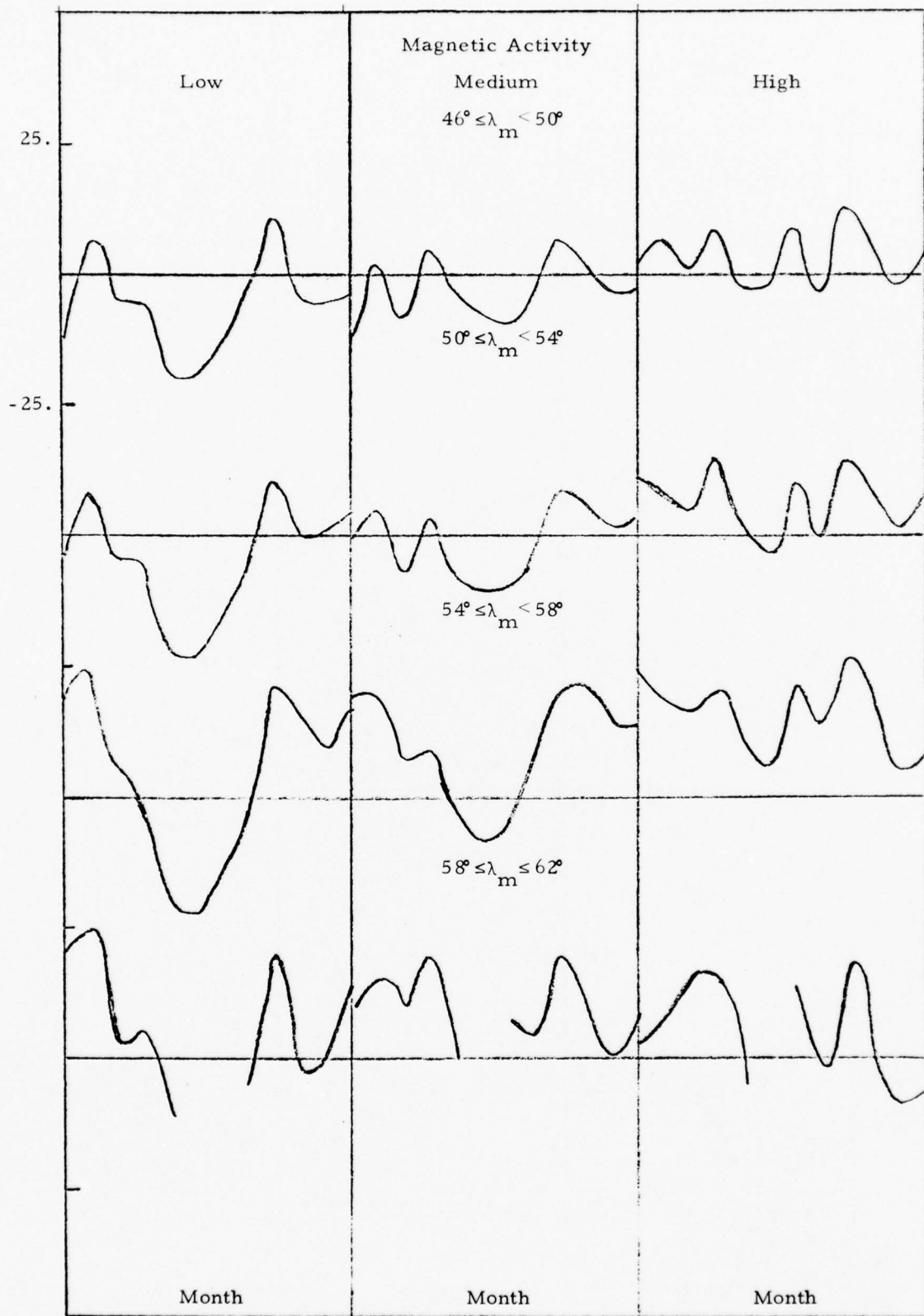


Figure I-8
18

AVERAGE PERCENT RESIDUAL: SOLAR DAY 1964

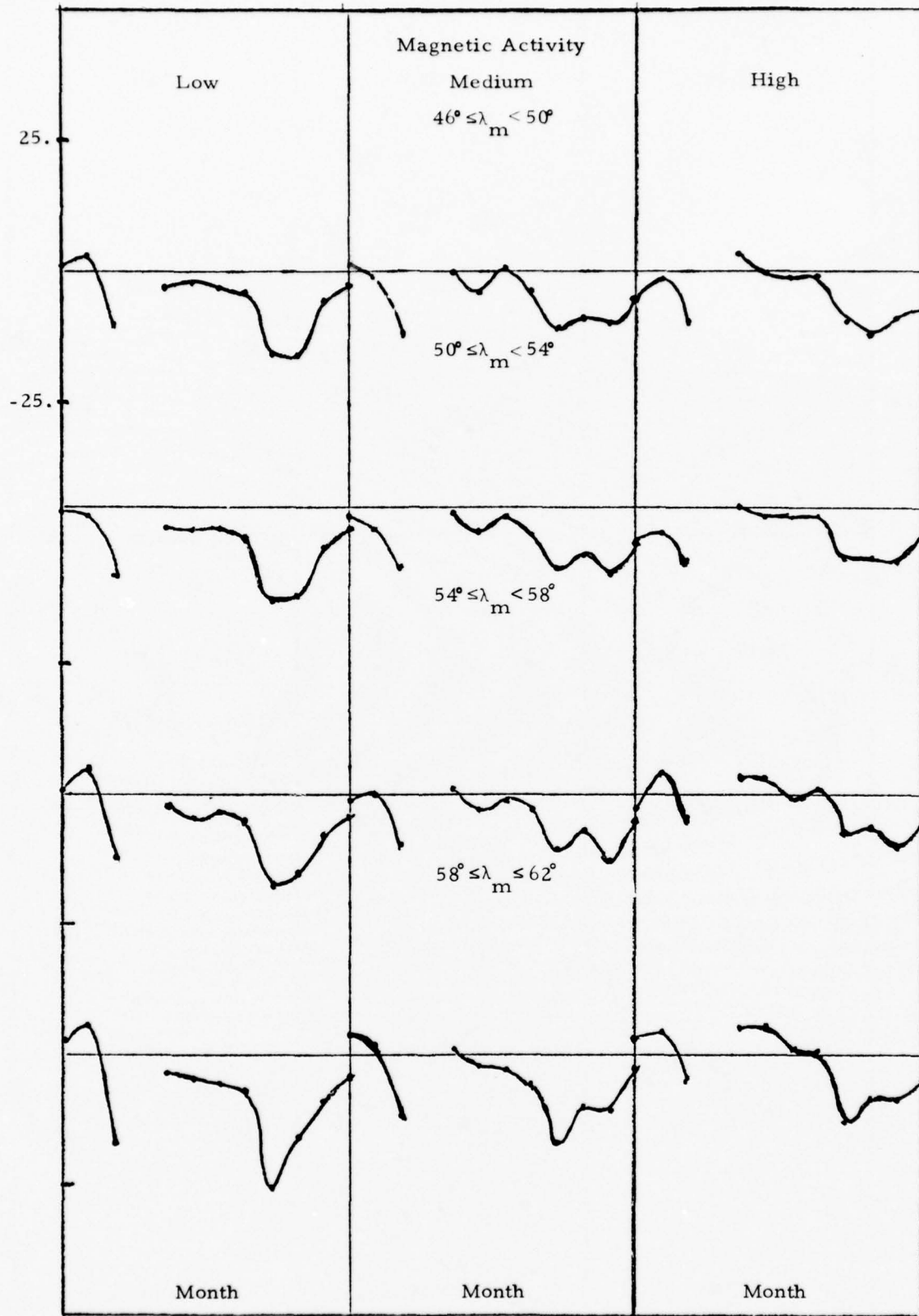


Figure I-9
19

AVERAGE PERCENT RESIDUAL: SOLAR NIGHT 1964

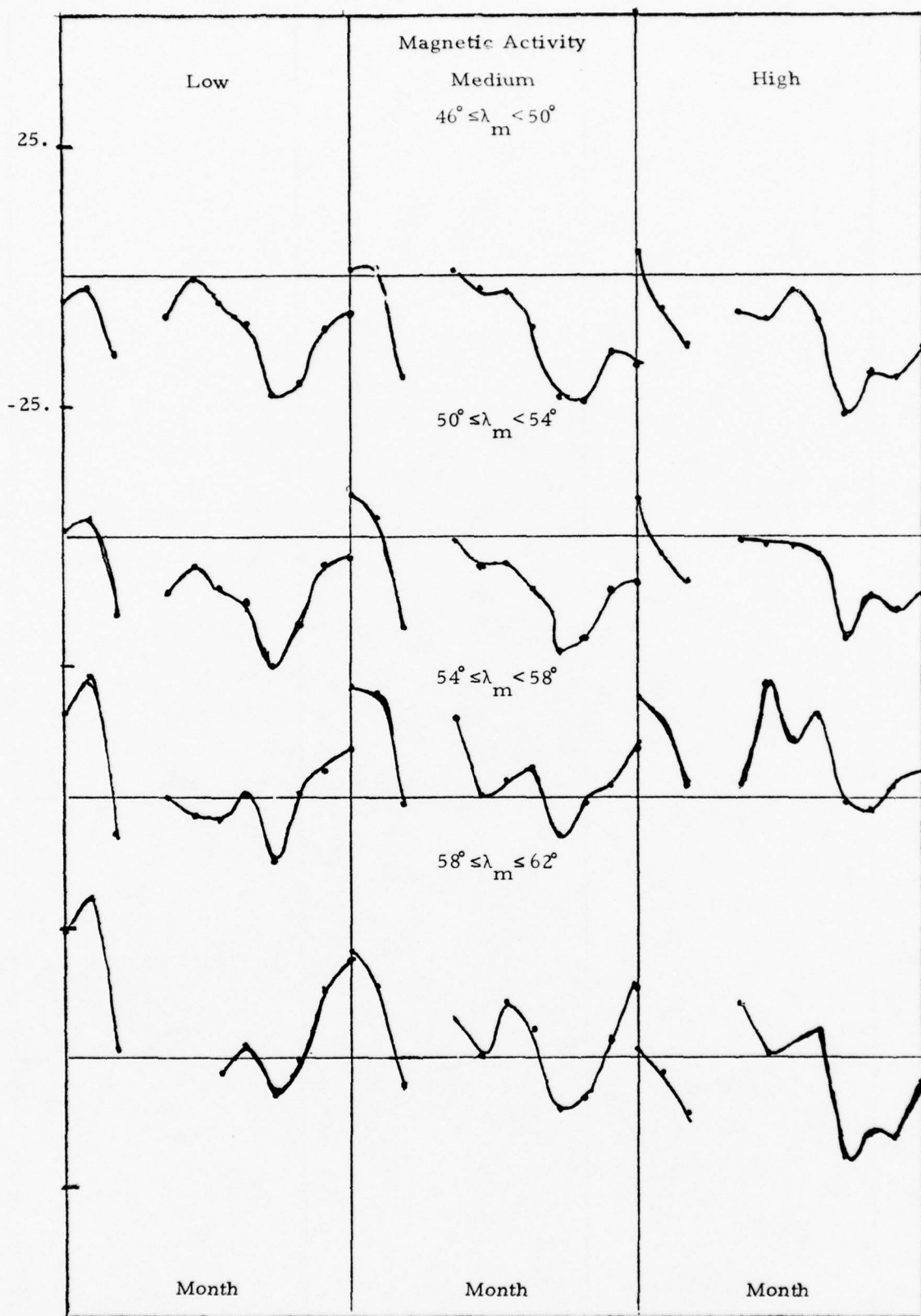


Figure I-10
20

AVERAGE PERCENT RESIDUAL: SOLAR DAY 1966

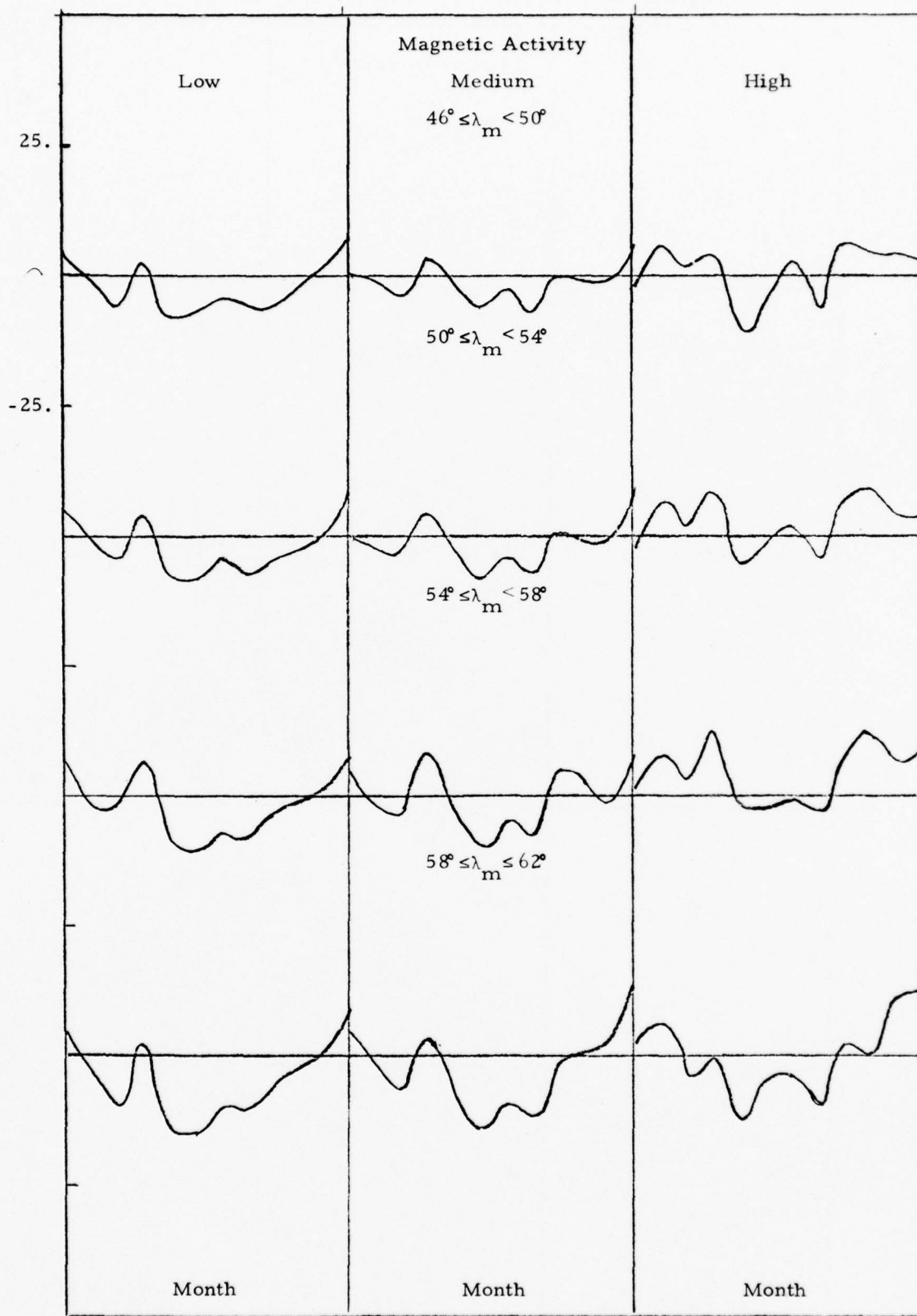


Figure I-11
21

AVERAGE PERCENT RESIDUAL: SOLAR NIGHT 1966

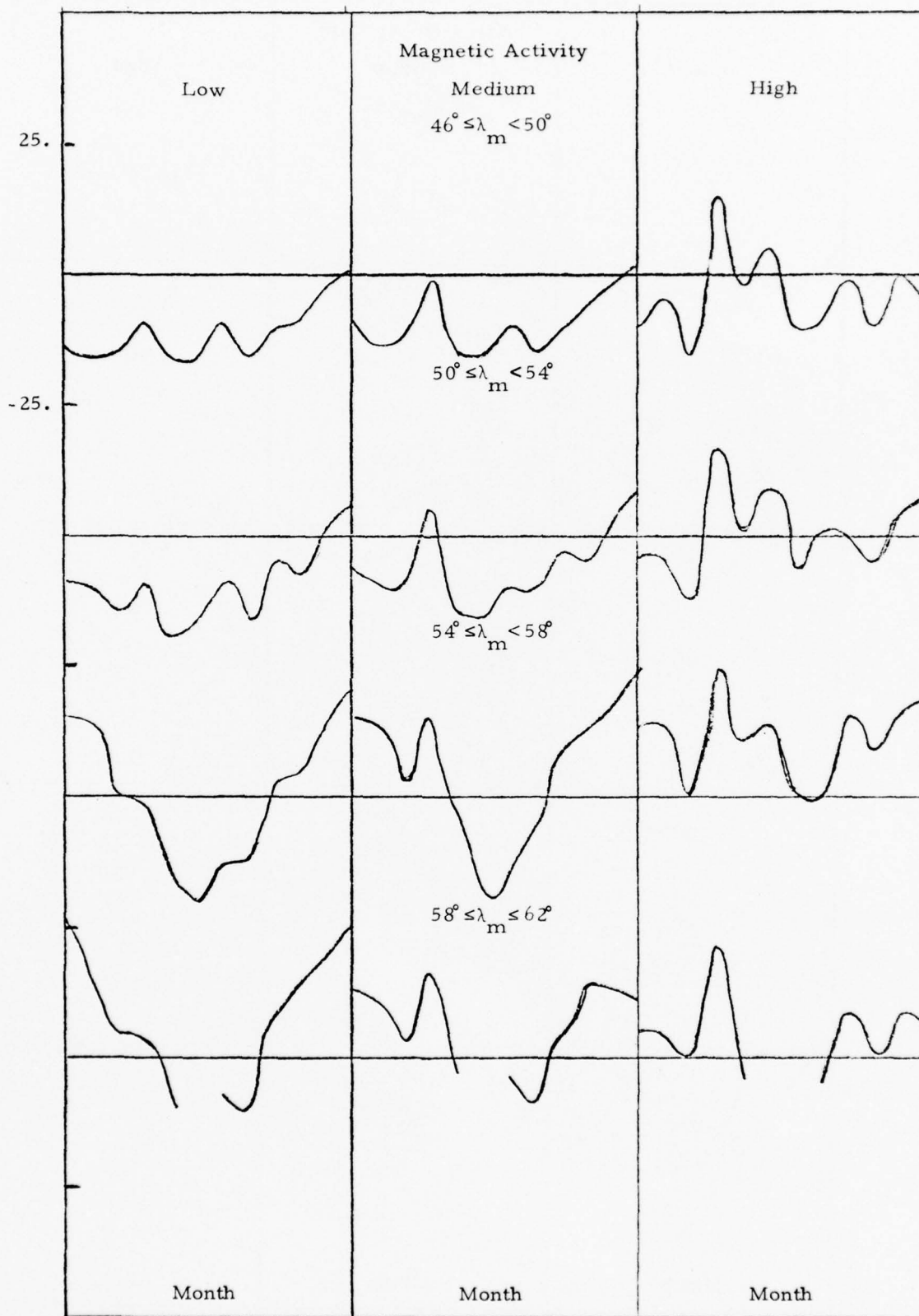


Figure I-12
22

AVERAGE PERCENT RESIDUAL: SOLAR DAY 1968

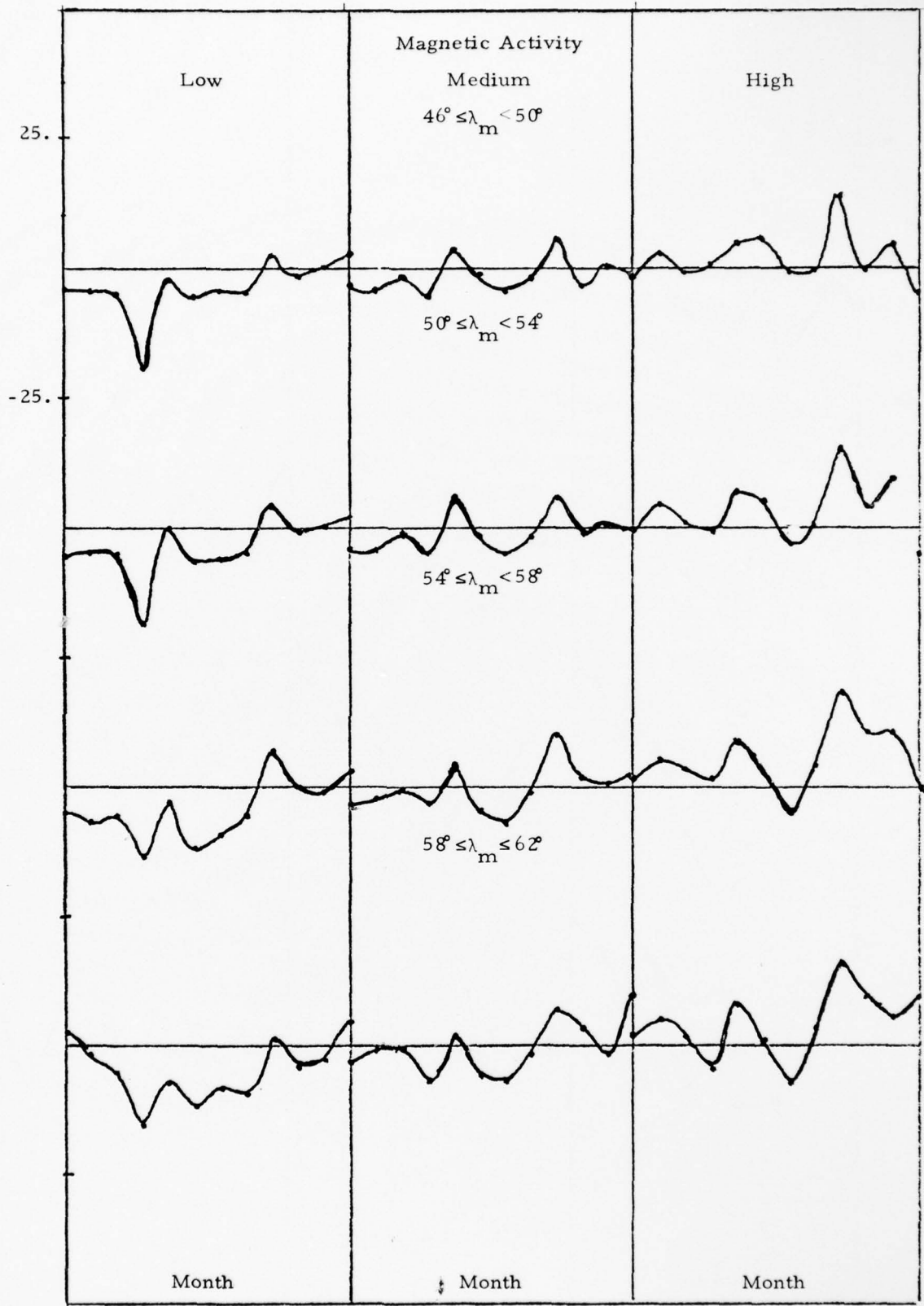


Figure I-13

AVERAGE PERCENT RESIDUAL: SOLAR NIGHT 1968

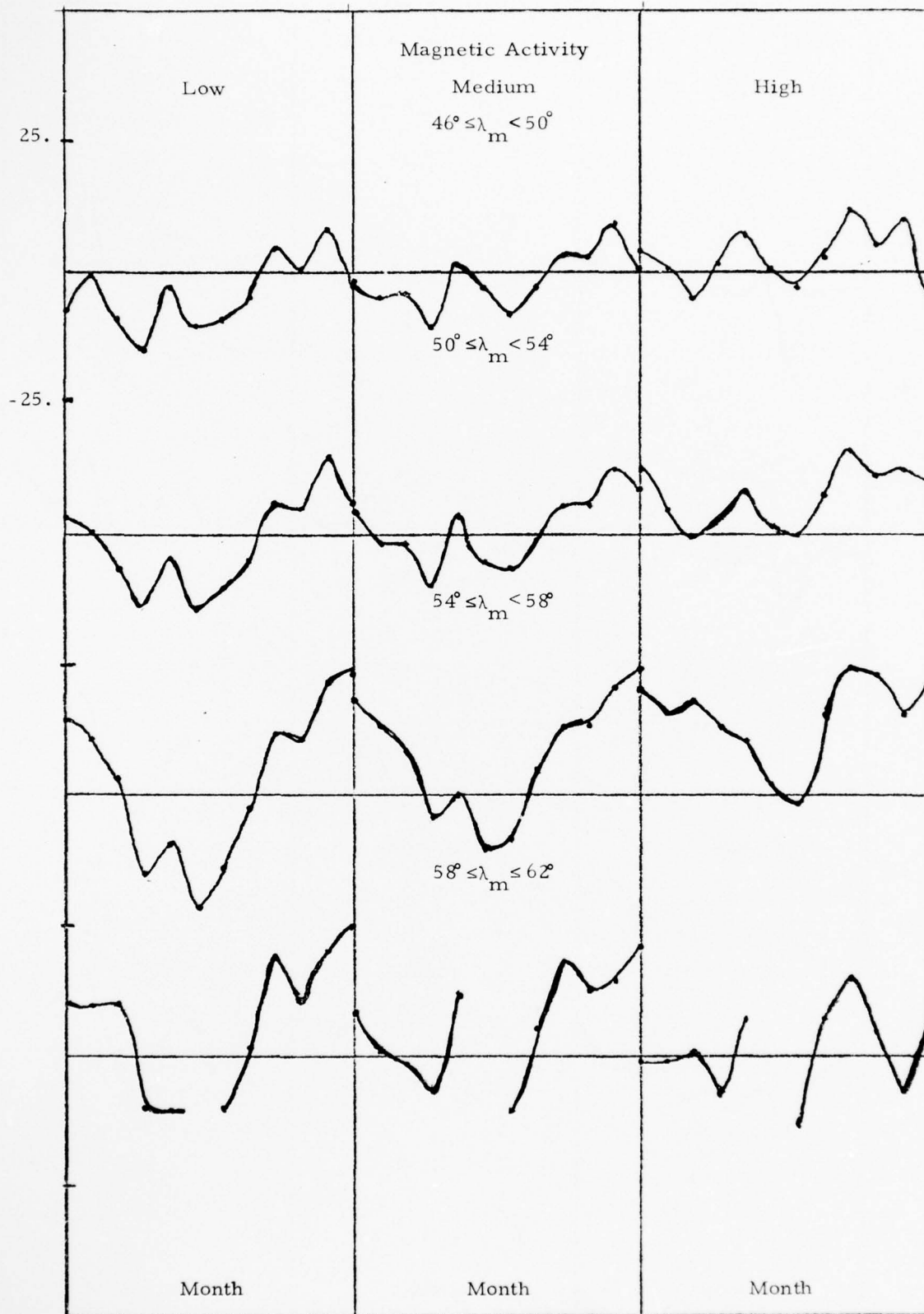


Figure I-14
24

for 1958. The daytime curves for the other years also show very little variation as a function of geomagnetic latitude. Since this data is confined to the region of $\lambda_m \leq 62^\circ$, there is no evidence in Δ due to the effect of the auroral oval.

In the curves for the solar night data, there is evidence of the existence of the high-latitude trough. Although it is not present in all years, it does show a strong seasonal dependence when it exists. This is most clearly seen in the data for 1968 where the ITS model predicts a value of foF2 which is approximately 25% too large in the winter months. The latitudinal dependence of the trough correction is also visible in the data, but appears to be only slightly correlated with magnetic activity. We have used this data to estimate the position, width and amplitude of the trough when it is observed. For a given K_p group, year and month the average residual was examined as a function of λ_m . For each month that shows a peak in $\Delta(\lambda_m)$, the center position, ϕ_T , the full width at one quarter maximum, Γ and the maximum amplitude, Δ_m was estimated. The results are presented in Table I-2 for the four years 1960, 1962, 1966 and 1968. The entries in each month for each of the years are close in value and the seasonal and K_p variation of the parameters is very similar. The solar-cycle dependence of foF2 appears to be adequately described by the ITS model since there is very little spread in the values of Δ_m for a given month. The width and center position along with other data were used to determine the position of the southern wall of the auroral oval as a function of corrected geomagnetic time.

We have combined all of these results in a set of corrections to be applied to the median model. In our previous work based on the 1958 data, we also noted an apparent linear dependence of the K_p correction during the solar day. In that data, there also seemed to be a seasonal dependence

TABLE I-2 High-Latitude Trough Parameters

		ϕ_T			Γ			Δ_M		
		L	M	H	L	M	H	L	M	H
January	1960	60°	58°	56°	4°	6°	4°	0.04	0.12	0.1
	1962	58	57	56	8	6	6	0.2	0.2	0.25
	1966	60	58	57	10	8	6	0.25	0.15	0.15
	1968	58	57	54	8	6	8	0.15	0.18	0.2
February		-	-	-	-	-	-	-	-	-
		58	57	56	10	6	6	0.2	0.2	0.2
		57	58	56	10	8	4	0.15	0.1	0.15
		58	56	56	12	4	4	0.1	0.12	0.16
March		-	-	56	-	-	4	-	-	0.07
		-	59	58	-	6	8	-	0.1	0.15
		-	-	-	-	-	-	-	-	-
		60	56	56	4	4	4	0.1	0.08	0.18
April		-	-	56	-	-	6	-	-	0.1
		-	60	56	-	6	10	-	0.2	0.1
		60	60	60	-	12	12	0.05	0.15	0.15
		-	-	56	-	-	4	-	-	0.12
May		-	-	-	-	-	-	-	-	-
		-	-	56	-	-	4	-	-	0.12
		-	64	56	-	4	4	-	0.08	0.1
		-	-	-	-	4	-	-	0.12	-
June		-	-	-	-	-	-	-	-	-
		-	-	56	-	-	4	-	-	0.08
		-	-	-	-	-	-	-	-	-
		-	-	-	-	-	-	-	-	-
July		-	-	58	-	-	10	-	-	0.1
		-	60	56	-	4	4	-	0.08	0.08
		-	-	-	-	-	-	-	-	-
		-	-	-	-	-	-	-	-	-
August		-	60	56	-	8	12	-	0.08	0.1
		-	57	56	-	4	4	-	0.06	0.14
		-	-	-	-	-	-	-	-	-
		-	58	56	-	-	12	-	0.05	0.15
September		-	-	55	-	-	10	-	-	0.1
		60	58	57	12	10	8	0.1	0.15	0.15
		64	57	57	10	10	10	0.1	0.10	0.15
		60	60	56	10	12	12	0.2	0.18	0.15
October		-	-	52	-	-	12	-	-	0.2
		56	56	56	4	6	6	0.15	0.2	0.2
		61	59	56	8	10	4	0.15	0.15	0.1
		60	58	55	12	12	6	0.12	0.12	0.23
November		60	52	52	12	10	10	0.08	0.1	0.15
		56	56	56	4	4	4	0.1	0.15	0.06
		60	58	57	10	8	8	0.2	0.17	0.17
		59	56	55	12	10	8	0.14	0.14	0.15
December		56	56	52	8	4	4	0.2	0.1	0.08
		58	56	55	8	6	6	0.15	0.15	0.1
		-	-	-	10	8	6	0.25	0.25	0.18
		58	58	56	10	8	8	0.25	0.25	0.22

of this correction. The data for the other years does not show this effect. The K_p correction was determined to be

$$\Delta(K_p) = -0.10 + 0.025 N_{gp}$$

and

$$foF2_A = foF2^{ITS} (1 - \Delta(K_p))$$

This correction of between -7.5% and +7.5% is applied independently of space and time to the model.

The spatial dependent features of the trough and auroral oval have been taken to be of the following form:

$$foF2 = foF2_A (1 + \Delta_N)$$

where $\Delta_N = A_o \sqrt{\exp} X_A \exp(-X_A^2/2)$ for $\lambda_m \geq \phi_A$

for the auroral oval

$$\phi_A = 71.9 - 2.5K_p - 5.1 \cos \left[\frac{\pi}{12} (t_{cgm} - 1) \right] \text{ (degrees)}$$

$$\phi_{mn} \leq \phi_A \leq \phi_{mx}$$

$$\phi_{mn} = 68.9 - K_p - 5.1 \cos \left[\frac{\pi}{12} (t_{cgm} - 1) \right]$$

$$\phi_{mx} = 70.9 - K_p - 5.1 \cos \left[\frac{\pi}{12} (t_{cgm} - 1) \right]$$

$$X_T = 7.0 - K_p \quad (\text{degrees})$$

$$4^\circ \leq X_T \leq 6^\circ$$

$$X_g = (\lambda_m - \phi_A) / X_T$$

$$X_A = 1.5 X_g$$

and for the trough

$$\Delta_N = T \left[1 + \cos \left(\frac{2\pi(D+31)}{365} \right) \right] \quad \text{for } \lambda_m < \phi_A$$

where $T = T_1 \sqrt{\exp} X_g \exp(-X_g^2/2) \exp(-(t_{cgm}-3)^2/12)$ for $|X_g| \leq 1$

$$T = T_1 \exp(-2.5(X_g-1)^2) \quad \text{for } |X_g| > 1$$

$$T_1 = 0 \quad \text{for } \chi \leq 90^\circ$$

$$\text{or } 6.0 < t_{cgm} < 18.0$$

$$T_1 = T_o \quad \chi > 94.6^\circ \quad \text{and} \quad t_{cgm} \leq 6.0 \quad \text{or} \quad t_{cgm} \geq 18.0$$

$$T_1 = T_o \frac{\chi - 90^\circ}{4.6^\circ} \quad 90^\circ \leq \chi \leq 94.6^\circ \quad \text{and}$$

$$t_{cgm} \leq 6.0 \quad \text{or} \quad t_{cgm} \geq 18.0$$

and where t_{cgm} is the corrected geomagnetic time. The maximum amplitudes have been taken to be $T_o = -0.20$ and $A_o = 0.20$. Examining

the five years data lead to the conclusion that only a small variation of the trough position and width should be contained in the corrections. This is contained in the above corrections by setting maximum and minimum values for ϕ_A and X_T . The limits on X_T and the functional form used allow the full width at one fourth maximum of the trough region to be between 6.3° and 9.5° .

The resulting model for foF2 was used to calculate the RMS residual for the same grouping of data as was done with the ITS model that was shown in Figure I-1 and I-2. Grouping the data according to solar day and night and month, 24 values of Δ_R were calculated. The number of months in which the new model showed an improvement over the ITS model is shown in the following table.

<u>Year</u>	<u>Solar Day</u>	<u>Solar Night</u>
1960	10	7
1962	11	10
1964	10	8
1966	9	10
1968	10	10

The use of the model depends upon having some prior knowledge of the activity in the polar region. During periods, such as 1958, in which the depression of foF2 due to the trough is particularly weak a smaller value

of the amplitude T_o should be used. When the model was applied to a small sample of polar stations measurements of foF2 made during 1969 and 1970, no significant improvement over the ITS model was made when a T_o of 20% was used.

REFERENCES

1. Miller, D.C. and Gibbs, J., (1975) Ionospheric Analysis and Ionospheric Modeling, AFCRL-TR-75-0549.
2. Jones, W.B. and Gallet, R.M., (1962) Representation of Diurnal and Geographic Variations of Ionospheric Data by Numerical Methods, ITU Telecomm. Jour. 29, (1962) 129.

II. STUDIES OF IONOSPHERIC RAY TRACING IN PARABOLIC IONOSPHERES WITH GRADIENTS

INTRODUCTION:

A fundamental problem in the design, planning, and operation of HF communications systems operating in the frequency range 2 to 30 MHz is to obtain realistic quantitative estimates of the expected long term performance of such systems. Such predictions are usually effected by ray tracing techniques through a realistic model of the ionosphere. In the general case, where realistic global electron density, magnetic field, and electron collision frequency models are taken into account, numerical integration of the Haselgrove equations,⁽¹⁾ such as described by Jones⁽²⁾, is generally required. Such an approach generally requires powerful computer facilities beyond the capability of field operations.

Other techniques generally employ a spherically symmetric electron density model neglecting the magnetic field. In such an ionosphere Bouguer's rule applies and the ray trace equations may be reduced to quadratures (see, for example Croft and Hoogasian⁽³⁾). These integrals have approximate solutions for the parabolic electron density model which were used by Barghausen et al⁽⁴⁾ to develop the ITS-78 operational parameter prediction program.

For certain simple ionospheres these integrals have exact solutions; the solution for the quasiparabolic ionosphere is described by Croft and Hoogasian⁽³⁾, the quasilinear case by Westover⁽⁵⁾.

These solutions, based on a spherically symmetric ionosphere, may be employed for cases where horizontal gradients exist in electron density if the effect of such gradients may be adequately represented by a displacement of the center of curvature of the spherically symmetric ionosphere from the center of the earth. The formal solution in such a situation is

described by Folkestad⁽⁶⁾. A method of determining the effective center of curvature based on variation of virtual height was developed by Beckwith⁽⁷⁾ as a basis of predicting propagation characteristics⁽⁸⁾.

Fundamental to all HF computer prediction programs is a synoptic numerical representation of the ionospheric characteristics. Typically, electron density models are developed by representing the ionosphere as one or more parabolic layers, the parameters of which (critical frequency, layer height and semithickness) are determined from global maps of coefficients⁽⁴⁾ or empirical functions representing diurnal, seasonal, and solar cycle variation. Implicit in these models are horizontal gradients in electron density due to variations in the layer parameters. It is useful to inquire into the effect of such gradients in the propagation characteristics of HF radio waves. In particular, it is useful to inquire as to whether the effects of such gradients may be reduced to a displacement of the center of curvature of an equivalent spherically symmetric ionosphere. If so, the formalism exists to develop a rapid, efficient and accurate algorithm for the prediction of propagation characteristics.

The present study is an investigation of the effects of gradients in the critical frequency. Numerical ray traces were calculated using the ARCON II 3D ray tracing program; a dipole approximation of the geomagnetic field was included with a simple parabolic electron density to represent the F2 layer. Ad hoc gradients, parallel and perpendicular to the ray direction, were included. The results of the calculation were compared to those derived from the analytic solution of the quasiparabolic electron density model. The rotation of the rays was investigated in its dependence on propagation characteristics, particularly the virtual height.

COORDINATE SYSTEMS AND MAGNETIC FIELD:

The ARCON II 3D Ray Tracing Program, as its predecessor the JONES 3D Ray Tracing Program, explicitly considers two coordinate systems: (1) The geographic coordinate system with the pole aligned with the axis of rotation of the earth and prime meridian passing through Greenwich, England, and (2) the geomagnetic coordinate system with pole aligned with the dipole magnetic pole, and prime meridian containing the geographic north pole. Input and output coordinates are generally referenced to the former, while internal calculations are referenced to the latter.

For ray-tracing applications wherein the geomagnetic field is ignored, the differences between the two is moot; similarly, when a simple isotropic model is employed for the electron density. However, when ray-tracing with magnetic field and a realistic global electron density model, ARCON II constrains the user to reference the electron density model, collision frequency model and geomagnetic field model to a single coordinate system. Specifically, the geomagnetic field model is the IGRF (1965)^(9,10) model referenced to the geomagnetic-dipole coordinate system; thus, the electron density must be referenced to this system.

It is often desirable for the computational coordinate system to be specified arbitrarily; in particular, ray tracing applications ultimately require range and azimuth of the salient features from the transmitter. Range and azimuth are the spherical coordinates of a coordinate system with pole at the transmitter and prime meridian containing the north geographic pole, * this coordinate system shall be referred to as the transmitter coordinate system (TCS), and is patently the natural coordinate system for the general ray tracing problem.

* In a right-handed coordinate system, the "longitude" coordinate is Π - azimuth.

One application where the use of the TCS is particularly desirable is in the present study of the effects of longitudinal and transverse gradients of the electron density on propagation characteristics. The TCS is the canonical coordinate system for this study; the desired perturbations to the electron density model may be modelled directly and simply; the resultant effects on propagation characteristics are also simply presented.

Another example is in using the numerical electron density model, the default model of ARCON II. Generally, a transmit site and coverage domain are predefined for the application, and a numerical ionosphere is generated sufficiently extensive to trace the required rays. Often, the required application is stated as a transmitter at a given geographic location covering a small azimuth domain to several thousand kilometers in range. In constructing the numerical ionosphere, the user must convert this information to an equivalent domain in geomagnetic coordinates. Usually, the desired coverage requires a considerable larger domain in geomagnetic coordinates than in the TCS; a considerable portion of the resulting array of plasma frequencies remains inactive during the ray trace, and the user may be constrained to use a larger grid spacing than he would otherwise deem desirable in order to limit core storage requirements. Use of the TCS in the ionosphere construction program precludes the requirement on the user to transform coordinates and allows for an ionosphere tailored to the application.

In conclusion, we submit that the TCS is the preferred coordinate system in most ray-tracing applications.

However, when the coordinate system for the ray tracing algorithm is arbitrarily specified, there remains the problem of the proper treatment of the geomagnetic field. The present geomagnetic field model is the IGRF

(1965) model referenced to the geomagnetic dipole coordinate system. It is undesirable in terms of execution efficiency to effect a coordinate transformation to the coordinate system of the geomagnetic field model every time the field components are desired. The solution of the problem is to rotate the components of the geomagnetic field and reference the field directly to the chosen computational coordinate system.

The geomagnetic field vector \vec{B} is given by

$$\vec{B} = - \text{grad } V, \quad (1)$$

where V is a scalar potential given by

$$V(r, \theta, \varphi) = \sum_{n=0}^B V_n(r, \theta, \varphi) \quad (2)$$

The partial potentials V_n are given by

$$V_n(r, \theta, \varphi) = r_o \sum_{m=0}^n (r_o/r)^{n+1} P_n^m(\cos \theta) \{g_n^m \cos m\varphi + h_n^m \sin m\varphi\} \quad (3)$$

where, r_o is the radius of the earth, r, θ, φ are the coordinates of the field point, the g_n^m and h_n^m are the expansion coefficients given by IAGA commission 2⁽¹⁾ in geographic coordinates and equivalently by Mead⁽²⁾ in geomagnetic dipole coordinates, and the P_n^m are the Schmidt quasi-normalized associated Legendre functions of degree n and m given by

$$P_n^m(X) = \left[\frac{\epsilon_m (n-m)!}{(n+m)!} \right]^{1/2} (1-X^2)^{m/2} \frac{d^{m+n}}{dX^{m+n}} (X^2-1)^n \quad (4)$$

where $\epsilon_m = 2$ for $m \geq 1$.

Consider the dipole terms ($n=1$) of equation (3):

$$V_1(r, \theta, \varphi) = (r_o/r)^3 (g_1^1 x + h_1^1 y + g_1^0 z) \quad (5)$$

where $x = r \sin \theta \cos \varphi$

$y = r \sin \theta \sin \varphi$

$z = r \cos \theta$

Equation (5) may be expressed in vector notation as

$$V_1(\vec{r}) = (r_o/r)^3 \vec{P} \cdot \vec{r} \quad (6)$$

where the components of the dipole moment vector \vec{P} are identified as

$$(P_x, P_y, P_z) \equiv (g_1^1, h_1^1, g_1^0) \quad (7)$$

Given the components of the dipole moment \vec{P} in the coordinate system \vec{r} , then the components in a rotated coordinate system

$$\vec{r}' = \vec{R} \cdot \vec{r} \quad (8)$$

are given by

$$\vec{P}' = \vec{R} \cdot \vec{P} \quad (9)$$

where \vec{R} is the rotation matrix transforming between the two coordinate systems. Equation (9), then, is the desired transformation of the dipole field to an arbitrary coordinate system.

The higher-order components of the geomagnetic field are elements of higher-rank tensors and may be transformed, in principle, by application of the rotation matrix. However, it may be more efficient computationally to take advantage of the scalar nature of the V_n and generate $2n+1$ simultaneous equations for the n^{th} order expansion coefficients. The latter approach was used by Mead⁽¹⁰⁾ to develop the values of the components in the dipole coordinate system.

In the ray-trace applications currently studied, the dipole approximation of the geomagnetic field is adequate; thus, only the transformation of the dipole terms given by equation (9) has been implemented for use in the ARCON II ray trace program. However, we hope to optimize the versatility of ARCON II in the near future by implementing an algorithm to rotate the higher order components of the geomagnetic field.

ELECTRON DENSITY MODEL:

The ambient ionosphere for this study was specified as a parabolic electron density model. The plasma frequency f_p in this model is given by

$$\begin{aligned} f_p^2 &= f_c^2 (1-y^2) \quad h_m - y < h < h_m + y \\ f_p &= 0 \quad \text{otherwise} \end{aligned} \quad (10)$$

where $y = (h-h_m)/y_m$

and f_c is the critical frequency, h_m the parabolic layer height of maximum electron density, y_m the layer semithickness, and h the altitude. For this study, h_m and y_m were fixed at 300 km and 100 km respectively, and the critical frequency f_c was taken nominally to be 10 Mhz. However, ad hoc gradients were allowed in f_c such that

$$f_c = f_{co} (1 + A (\theta - \theta_o) + B \sin \theta (\varphi - \varphi_o)) \quad (11)$$

where $f_{co} = 10$ MHz, A and B are ad hoc gradients, θ is range from the transmitter and φ is the azimuth of the ray point from the receiver.

Since the actual variability of $f_o F_2$ is generally less than 10 MHz over 30 degrees, values of A and/or B less than 2 (with $f_{co} = 10$ MHz and θ, φ in radians) suffice to simulate typical ionospheric conditions. Sets of ray traces were computed for A and/or B equal to 0, 1, and 2.

Since it was desired that the nominal electron density profile (i. e. $f_c = 10$ MHz.) obtain at or near the ray reflection point, the reflection point (θ_o, φ_o) must be estimated prior to tracing each ray. Since the azimuthal deviations were small (generally less than 2 degrees), φ_o may be taken as the initial takeoff azimuth. The nominal range θ_o was then estimated from virtual height analysis appropriate to parabolic layer theory.

The ray geometry is shown in Figure 3. Parabolic layer theory gives the virtual height h_v at operating frequency f and takeoff elevation β_o as,

$$h_v = h_b + \frac{1}{2} y_m u \log \left(\frac{1+u}{1-u} \right) \quad (12)$$

where,

$$h_b = h_m - y_m ,$$

and,

$$u = (f/f_c) \sin \beta_v ; \quad (13)$$

while β_v is the local elevation angle of the unrefracted ray at the apex of the virtual triangle and is given by,

$$\cos \beta_v = (r_o/r_v) \cos \beta_o . \quad (14)$$

where r_o is the radius of the earth, and $r_v = r_o + h_v$.

Equations (12) to (14) patently require iteration for the solution h_v ; starting from the initial estimate $h_v = h_b$ two iterations were

considered sufficient to estimate the range θ_o to the reflection profile given by,

$$\theta_o = \beta_v - \beta_o \quad . \quad (15)$$

This technique located the reflection profile to better than 4 kilometers in most cases for the control ionosphere (no gradients and no magnetic field). Larger errors only occurred at elevations close to the skip distance elevation; however, all deviations were less than 16 kilometers at elevations less than the skip elevation.

When gradients and magnetic field were introduced, the actual points at which reflection occurred never deviated from the estimated profile by more than 100 kilometers; the deviations exceeded 32 kilometers only near the skip distance elevation at frequencies exceeding 25 MHz. Thus, the critical frequency at the reflection point never differed from the nominal value of 10 MHz by more than 5%, and generally by much less than 1%.

THE QUASIPARABOLIC ELECTRON DENSITY MODEL (QP MODEL)

The QP Model has considerable utility as an initial approximation to the ray traces in the ionospheres under consideration, primarily because it yields analytic expressions for ray traces through this model ionosphere as shown by Croft and Hoogasian.⁽³⁾ The QP Model has been used by Rao⁽¹¹⁾ to develop a method of extracting ionospheric parameters from measured minimum group paths at a set of frequencies.

The QP Model gives the plasma frequency $f_p(r)$ in terms of ionospheric parameters of a single layer ionosphere, to wit, critical frequency f_c , layer altitude h_m , and semithickness y_m .

$$\begin{aligned} f_p(r) &= f_c \left[1 - y^2 \right]^{\frac{1}{2}} \quad , \quad r_b < r < r_m \quad r_b/(r_b - y_m) \\ f_p(r) &= 0 \quad \text{otherwise} \end{aligned} \tag{16}$$

where $y = (r_b/r) \cdot (r - r_m)/y_m$, $r_m = r_0 + h_m$,

$r_b = r_m - y_m$, and r_0 is the radius of the earth.

The ray trace solutions derived by Croft and Hoogasian⁽³⁾ are shown as families of group path and range as functions of takeoff elevation in Figures 1 and 2 respectively. The parameters of the QP Model used were $r_0 = 6370$ km, $f_c = 10$ MHz, $h_m = 300$ km, and $y_m = 100$ km.

Each curve is for a constant f_T/f_c where the transmitter frequency, f_T , varies between 2 and 30 MHz in 2 MHz steps.

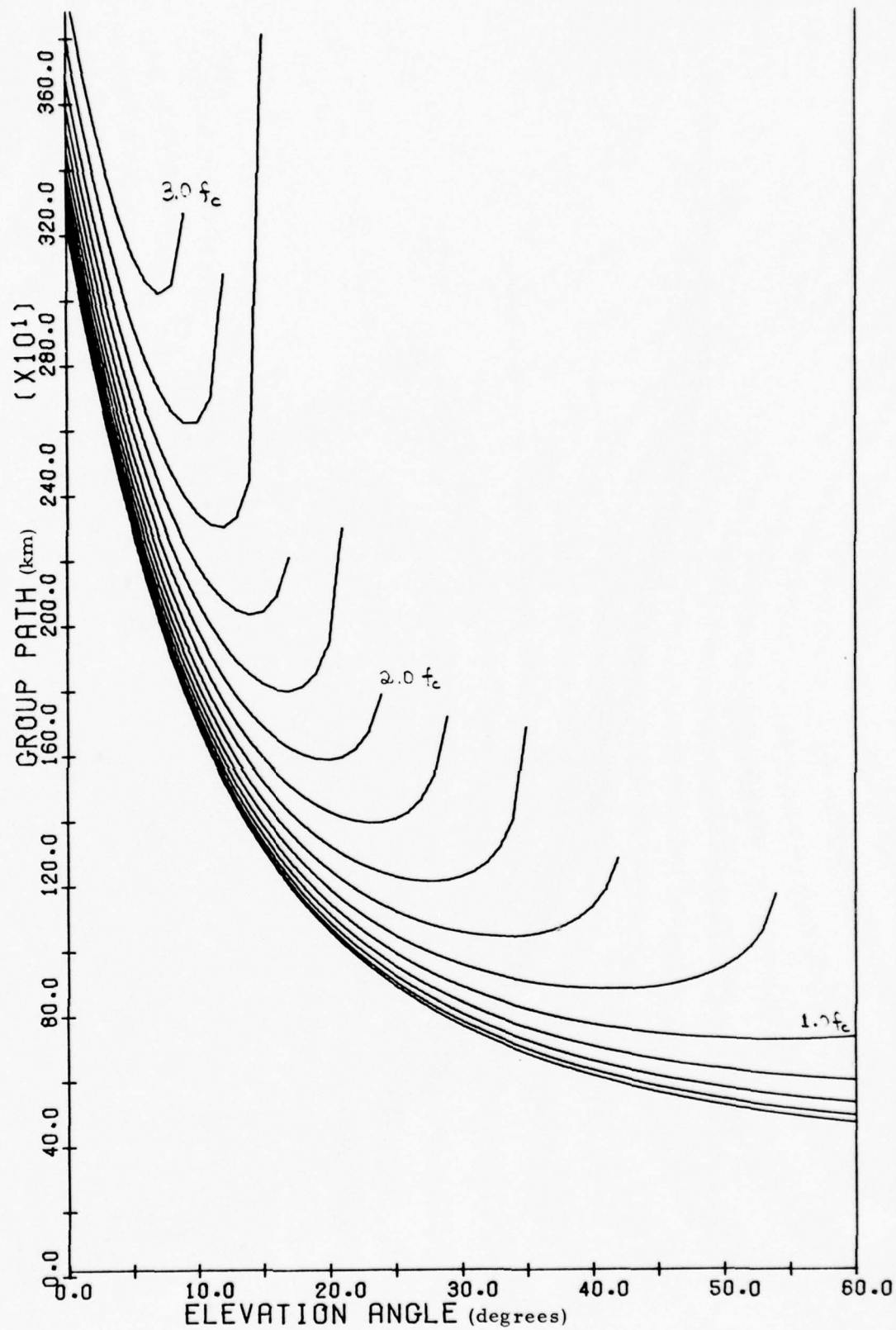


Fig. 1. Group Path Length vs. Elevation with Frequency as a Parameter

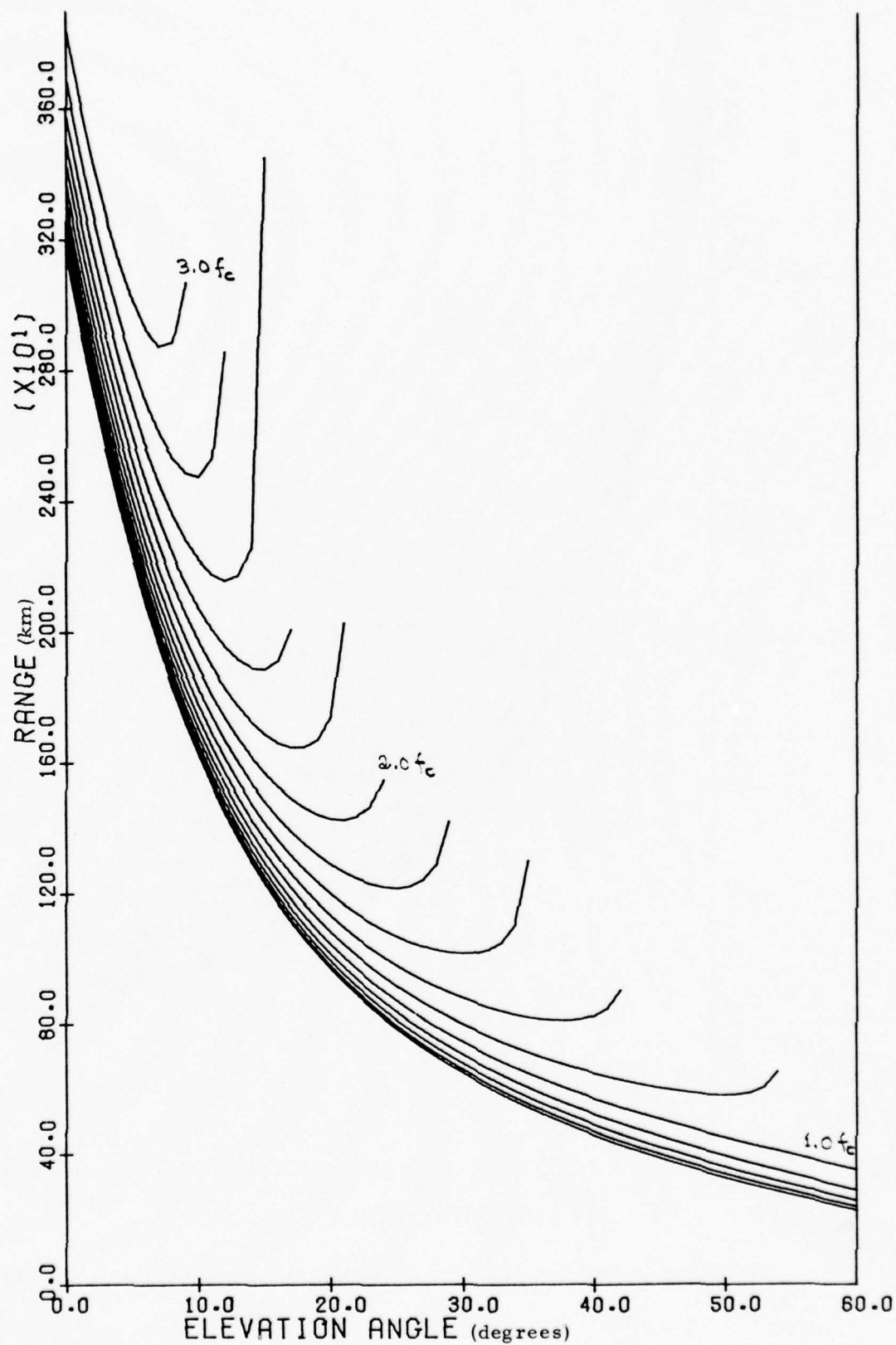


Fig. 2. Ground Range vs. Elevation with Frequency as a Parameter

Our objective is to use knowledge of the ionosphere in lieu of precise knowledge of elevation angle to determine ground range from a measured group path at a given frequency. Thus, we need to enter Figure 1 at a given group path and frequency, extract an elevation angle and enter Figure 2 for range; in short, we desire to invert the functions of Figure 1. To do so efficiently, we analyzed the solutions of Croft and Hoogasian, simplified the functional forms, and chose a convenient variable with which to represent the solution.

The ground-to-ground, one-hop group path P' is given by

$$P' = 2r_b \sin \gamma_p (G_F + G_I) \quad (17)$$

where r_b (previously defined) is the base of the ionosphere, γ_p is the maximum entry angle above which all rays at that frequency will penetrate the ionosphere, G_F is the contribution from the free space propagation (transmitter to bottom of ionosphere), and G_I is the contribution from integration within the ionosphere (bottom of ionosphere to ray apogee). The contributions G_F and G_I are given by:

$$\begin{aligned} G_F(z) &= z - z' \\ G_I(z) &= G_1 \left[G_2 \log \left(\frac{1+z}{1-z} \right) - z \right] \end{aligned} \quad (18)$$

where, with the ray geometry of Figure 3,

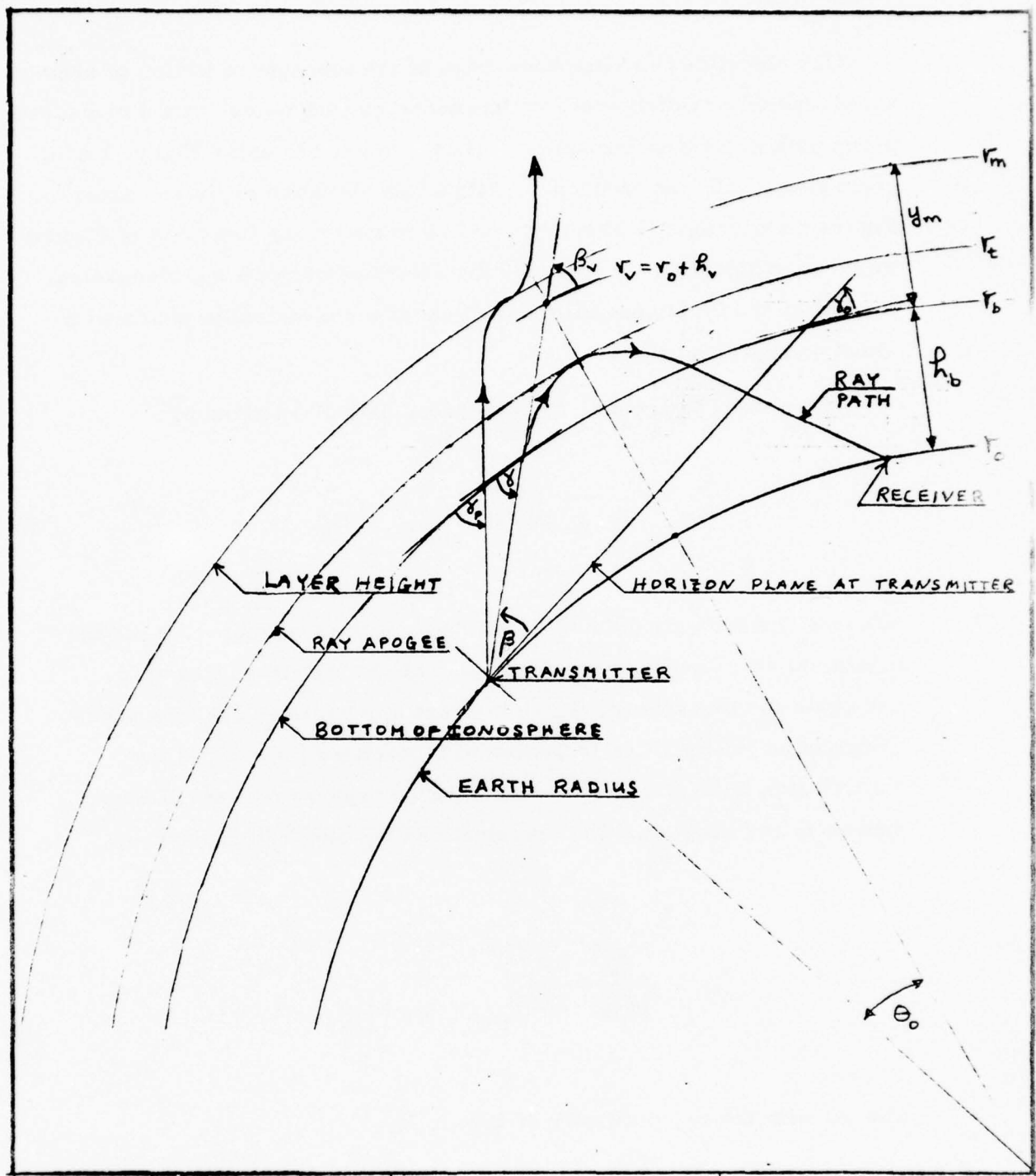


Fig. 3. Ray Geometry (not to scale)

$$z = \sin\gamma / \sin\gamma_p$$

$$z' = \cos\gamma_0 \cdot \sin\beta / \sin\gamma_p = (z^2 - z_0^2)^{1/2}$$

$$\cos\gamma_0 = r_0 / r_b$$

$$\cos\gamma = \cos\gamma_0 \cos\beta$$

$$z_0 = \sin\gamma_0 / \sin\gamma_p \quad . \quad (19)$$

The constants G_1 , G_2 and $\sin\gamma_p$ depend upon the transmitter frequency f and are given by

$$G_1 = F^2 / A$$

$$G_2 = B / 2B'$$

$$\sin\gamma_p = B' / F \sqrt{A} \quad (20)$$

where,

$$F = f / f_c$$

$$F_m = (r_m / y_m)^{1/2}$$

$$B = F_m^2 (F_m^2 - 1)$$

$$B' = F_m^2 - F^2$$

$$A = B - B' \quad . \quad (21)$$

Note that at $F = F_m$, $\gamma_p = 0$; thus, F_m is the maximum (scaled) frequency for which the QP model ionosphere will support reflections. However, in ground to ground transmission γ_p can be no less than γ_0 ; accordingly, the maximum (scaled) reflecting frequency F_{\max} is considerably less than F_m , and is determined from γ_0 , which yields,

$$F_{\max} = F_m \left[\alpha - \sqrt{\alpha^2 - b^2} \right]^{\frac{1}{2}} \quad (22)$$

where

$$\alpha = 1 + \frac{1}{2} (F_m \tan \gamma_0)^2$$

$$b = \sec \gamma_0 \quad . \quad (23)$$

To determine the minimum group path at a given frequency, it is necessary to solve the equation,

$$G_z \equiv \partial G / \partial z = 1 - z/z' + 2G_1 G_2 / (1 - z^2) - G_1 = 0 \quad . \quad (24)$$

Although equation (24) reduces to a cubic in z^2 , thus permitting a solution in closed form, it is as effective numerically to employ a Newton iterative method, for which the second derivative of G is required, and given by,

$$G_{zz} \equiv \partial^2 G / \partial z^2 = ((z/z')^2 - 1)/z' + 4G_1 G_2 z / (1 - z^2)^2 \quad . \quad (25)$$

Solutions of equation (24) obtain for all $F < F_{\max}$ at z between z_0 and unity, favoring the upper limit. Thus, the iterative procedure is started from

$$z_m^{(0)} = 0.8 + 0.2 z_0^2 \quad (26)$$

and the solution z_m taken as the limit of the series

$$z_m^{(n)} = z_m^{(n-1)} - G_z / G_{zz} \quad (27)$$

With the salient features of the group path-elevation curve at a given frequency thus established, equation (17) may now be inverted for elevation, given group path. A unique solution exists in $z_0 < z < z_m$ if the input frequency is less than F_{\max} , and the given group path is between the minimum group path and the group path at $z = z_0$. Since equations (18) are intrinsically irrational, an iterative technique is mandated. From Figure 1, it is clear that a good first estimate $z^{(0)}$ to the low angle solution can be obtained by first subtracting from the given group path the excess ΔP over specular reflection from the base level at elevation $\beta = 0$, and treating the remainder as specular reflection (see Figure 4.). Therefore, if P' is the given group path at frequency f ,

then write

$$P' \equiv 2r_o \sin \gamma_p \{g + G_I(z_o)\}$$

$$G_p = P' / 2r_o \sin \gamma_p \quad .$$

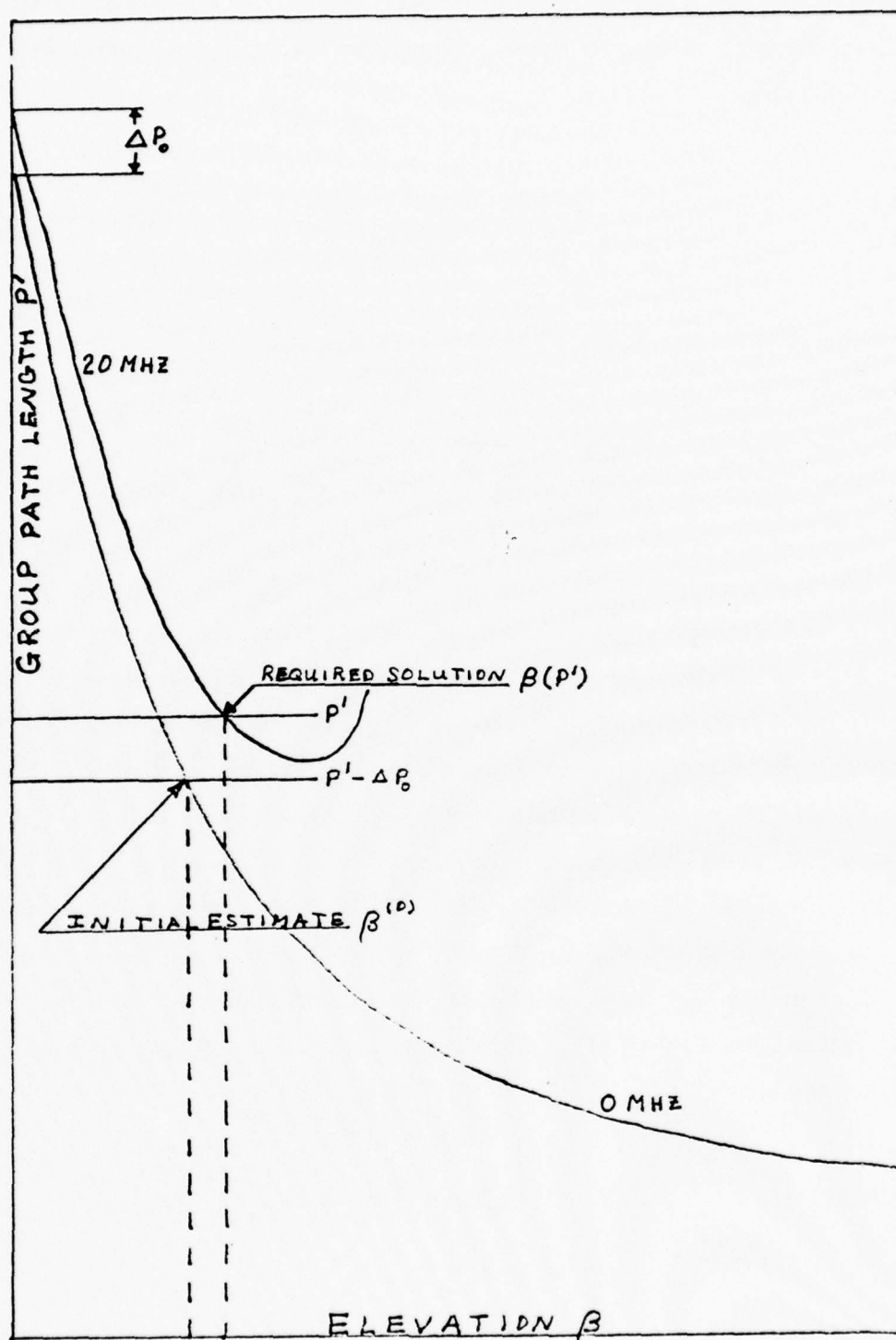


Fig. 4. Initial Estimation for Iterative Inversion of Group Path Length vs. Elevation Curve of Figure 1.

identify

$$g \equiv G_F(z^{(0)})$$

from which

$$z^{(0)} = \frac{1}{2} \{g + (z_o/g)^2\} \quad (28a)$$

If the high-angle solution is desired, the initial estimate may be taken between that for minimum group path z_m and penetration:

$$z^{(0)} = (1 + z_m)/2 \quad (28b)$$

The solution Z is taken as the limit of the series

$$z^{(n)} = z^{(n-1)} + [G_p - G(z^{(n-1)})]/G_z \quad (29)$$

From this solution the entry angle γ , takeoff elevation β , ground range D and penetration depth Δ are given by

$$\gamma = \sin^{-1}(z \sin \gamma_p)$$

$$\beta = \cos^{-1}(\cos \gamma / \cos \gamma_o)$$

$$D = 2r_o [(\gamma - \beta) + (\cos \gamma / \sqrt{4c}) \log W]$$

$$\Delta = r_b (B'/A) [1 - \sqrt{1 - z^2}] \quad (30)$$

where

$$C = B + B' + (Fz \sin \gamma_p)^2$$

$$W = [1 + \sqrt{C/A} z + (B'/A) z^2]^2 / [1 - z^2] \quad (31)$$

DATA FILES GENERATED BY THE NUMERICAL RAY TRACE

Six files containing results from the ARCON II 3D ray tracing program for frequencies from 2 to 30 MHz and elevations 2° to 45° (or penetration) were created for further statistical study. Parameters kept fixed for all files are listed in Table I, while Table II lists elements that were changed from file to file. A record was generated for each ray traced consisting of the basic coordinate data of the ray at the following points: transmitter, entry to ionosphere, ray apogee, exit from ionosphere, and ground reflection. In addition, information identifying the ray such as frequency, elevation, and information identifying the ionosphere was appended.

Table I: Fixed Ray Trace Parameters, All Files

TRANSMITTER LATITUDE:	45° N
TRANSMITTER LONGITUDE:	68° W
TAKEOFF AZIMUTH:	045°
ELEVATION RANGE:	0° to 45° , or penetration
ELEVATION STEP:	1°
FREQUENCY RANGE:	2 MHz to 30 MHz
FREQUENCY STEP:	2 MHz
INTEGRATION STEP SIZE:	0.25 km
MODEL IONOSPHERE:	Parabolic
NOMINAL CRITICAL FREQUENCY:	10 MHz
LAYER HEIGHT:	300 km
SEMITHICKNESS:	100 km

TABLE II: VARIED RAY TRACE PARAMETERS

<u>FILE NUMBER</u>	<u>FIELD MODEL</u>	<u>LONGITUDINAL GRADIENT (A)</u>	<u>TRANSVERSE GRADIENT (B)</u>
1	NONE	0	0
2	DIPOLE	0	0
3	DIPOLE	1	0
4	DIPOLE	2	0
5	DIPOLE	0	1
6	DIPOLE	0	2

ANALYSIS OF RESULTS:

The results of ray traces through the ionospheres with longitudinal gradients in the critical frequency were analyzed to discover correlations between deviations in range and group path from the predictions of the unperturbed quasiparabolic electron density model.

The control set of ray traces, no field and no gradients in critical frequency, yielded results from the numerical solution of the Haselgrove equations substantially in agreement with the analytical solution of the quasiparabolic model; the root mean square deviations of the differences in range and/or group path length between the two were of the order of the integration step size (0.25 kilometers).

The essential effect of turning on the (dipole) magnetic field was to introduce a certain amount of "noise" in the ray trace results although systematic frequency dispersion is apparent. At frequencies exceeding two megahertz, the root mean square deviations in range and group path from the QP solution were less than 11 kilometers. At two megahertz, the RMS deviation was less than 20 km. Figure 5 shows the range deviations as functions of group path length. The subsets for frequencies 2, 4, 6 MHz, etc. are indicated by characters B, D, F etc. Significant range deviations occur primarily at low frequencies (2 and 4 MHz, when the gyrofrequency is significant compared to the operating frequency), and at other frequencies near the minimum group-path length.

The additional effects of longitudinal gradients in the critical frequency are shown in Figure 6 ($A = 1$) and Figure 7 ($A = 2$). No significant effect is noticed in either case at 2 and 4 megahertz; at higher frequencies the gradient effect tends to dominate over the magnetic field effect. A definite frequency dispersion is evident in these range deviations although patently

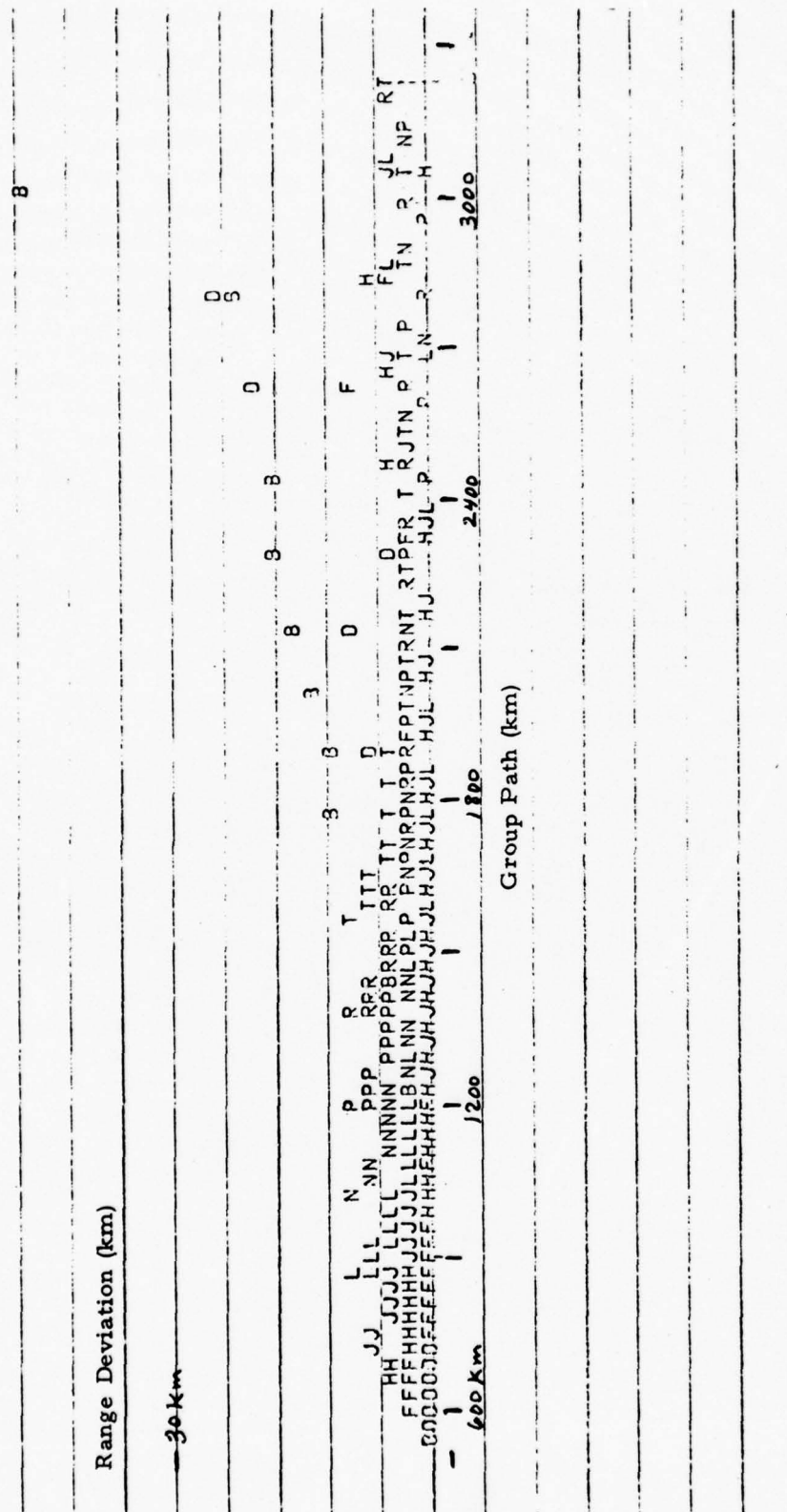


Fig. 5. Range Deviations from Quasiparabolic Solutions vs. Quasiparabolic Group Path Length. Case (a), Dipole Field-no Gradients.

BEST AVAILABLE COPY

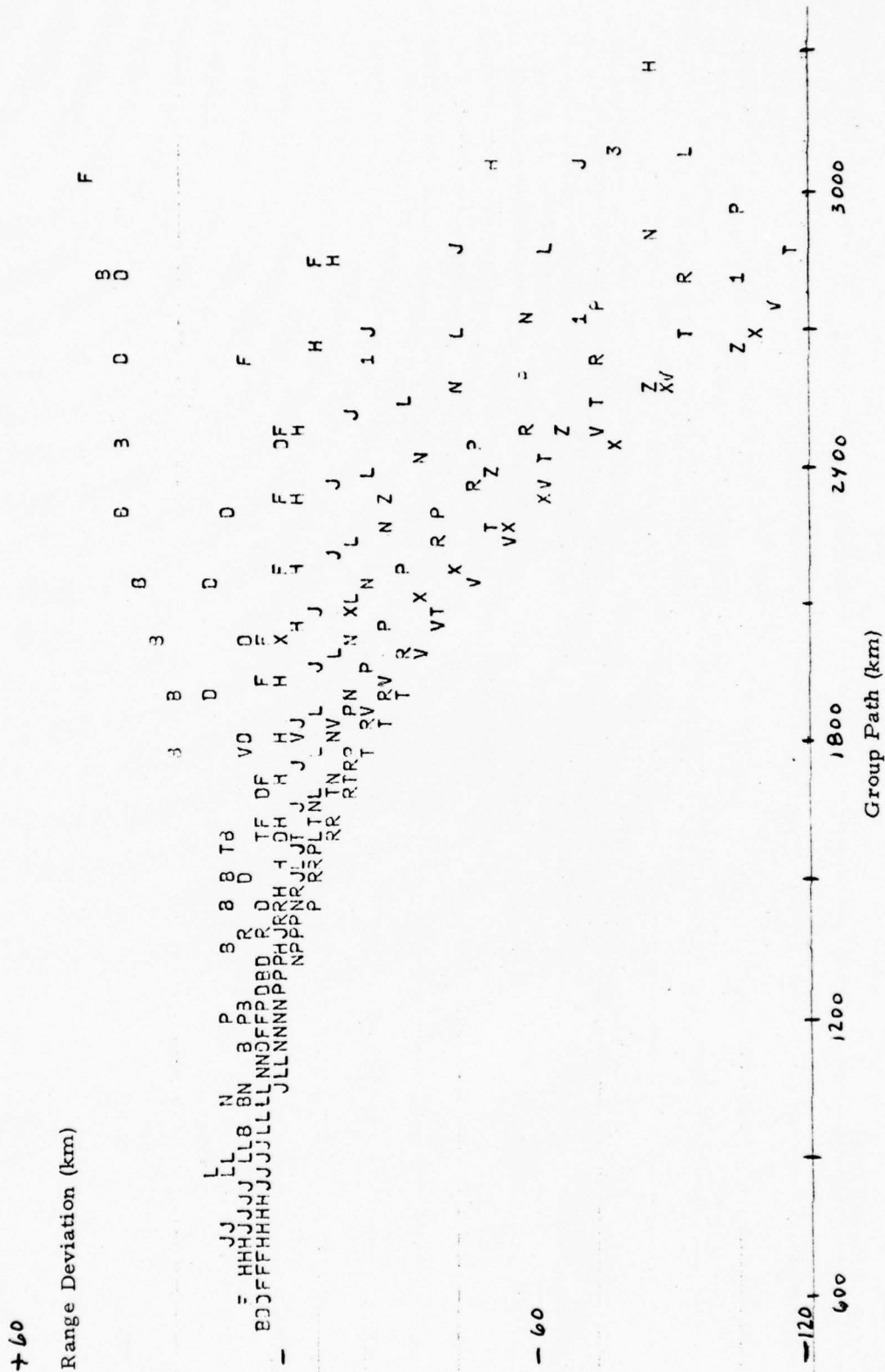


Fig. 6. Range Deviations, Dipole Field-longitudinal Gradient ($A=1$)

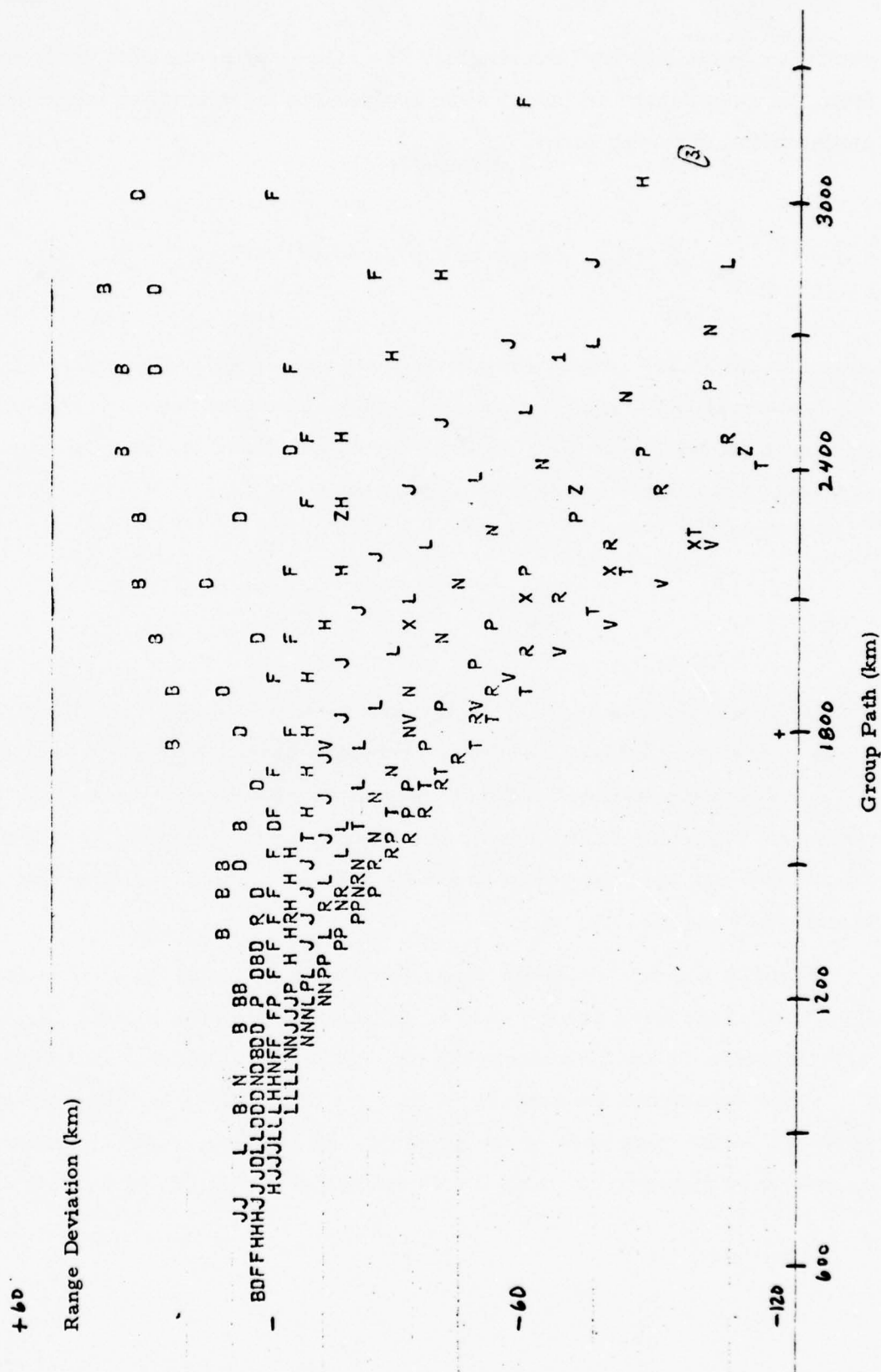


Fig. 7. Range Deviations, Dipole Field-longitudinal Gradient ($A=2$)

nonlinear in total group path length. The range and group path deviations from the quasiparabolic model were analyzed in an attempt to construct a model of the following form

$$R = R_{QP} + a(f, A) + b(f, A) (P' - P'_{QP}) \quad (32)$$

where R and P' are ground range and group path length as calculated from the numerical ray trace, R_{QP} and P'_{QP} are calculated from the quasiparabolic model, while $a(f, A)$ and $b(f, A)$ are functions of frequency and longitudinal gradient of critical frequency f_c

$$A = \frac{1}{f_c} \frac{\partial f_c}{\partial \theta}$$

Table III lists the results of this statistical analysis giving the fitting parameters a and b together with the standard deviations σ for $A = 1$ and 2 . A moderately well defined frequency dispersion in $a(f)$ is readily apparent (Figure 8) and appears to be directly proportional to A . On the other hand $b(f)$ appears not to be a well defined function of frequency, but statistically independent of A .

Figures 9 and 10 show the range deviations as functions of group path length for transverse gradients in critical frequency ($B = 1$ and 2 respectively), while Figures 11 and 12 present the corresponding azimuthal deviations. Each pair reinforces the conjecture that gradient effects are directly proportional to the magnitude of the gradient. In addition, range deviations appear to be strongly correlated with azimuthal deviations while both are

TABLE III: Fit of range deviations to group path
deviations for the ionospheres with
longitudinal tilt.

Frequency	a(f)	A=1 b(f)	$\sigma(f)$	a(f)	A=2 b(f)	$\sigma(f)$	A=0 RMS
2	0.14	1.00	0.12	0.12	1.00	0.13	19.
4	-0.20	1.00	0.22	-0.30	1.00	0.29	10.
6	-0.48	0.99	0.49	-0.80	0.97	0.62	5.
8	-1.03	0.97	0.84	-1.70	0.98	1.26	6.
10	-1.97	0.97	1.66	-3.39	0.96	2.61	8.
12	-4.14	0.93	3.97	-7.87	0.91	6.90	10.
14	-7.68	0.84	8.97	-14.31	0.83	13.67	10.
16	-9.79	0.82	10.75	-18.08	0.83	15.97	9.
18	-9.42	0.90	8.36	-16.74	0.90	12.16	10.
20	-13.93	0.86	11.79	-24.20	0.87	16.14	11.
22	-13.79	0.91	9.41	-24.25	0.91	12.89	
24	-20.78	0.88	12.87	-36.83	0.88	17.38	
26	-25.85	0.89	13.06	-50.42	0.86	19.54	
28	-30.43	0.91	11.12	-69.61	0.85	20.76	
30	-44.52	0.90	11.18				

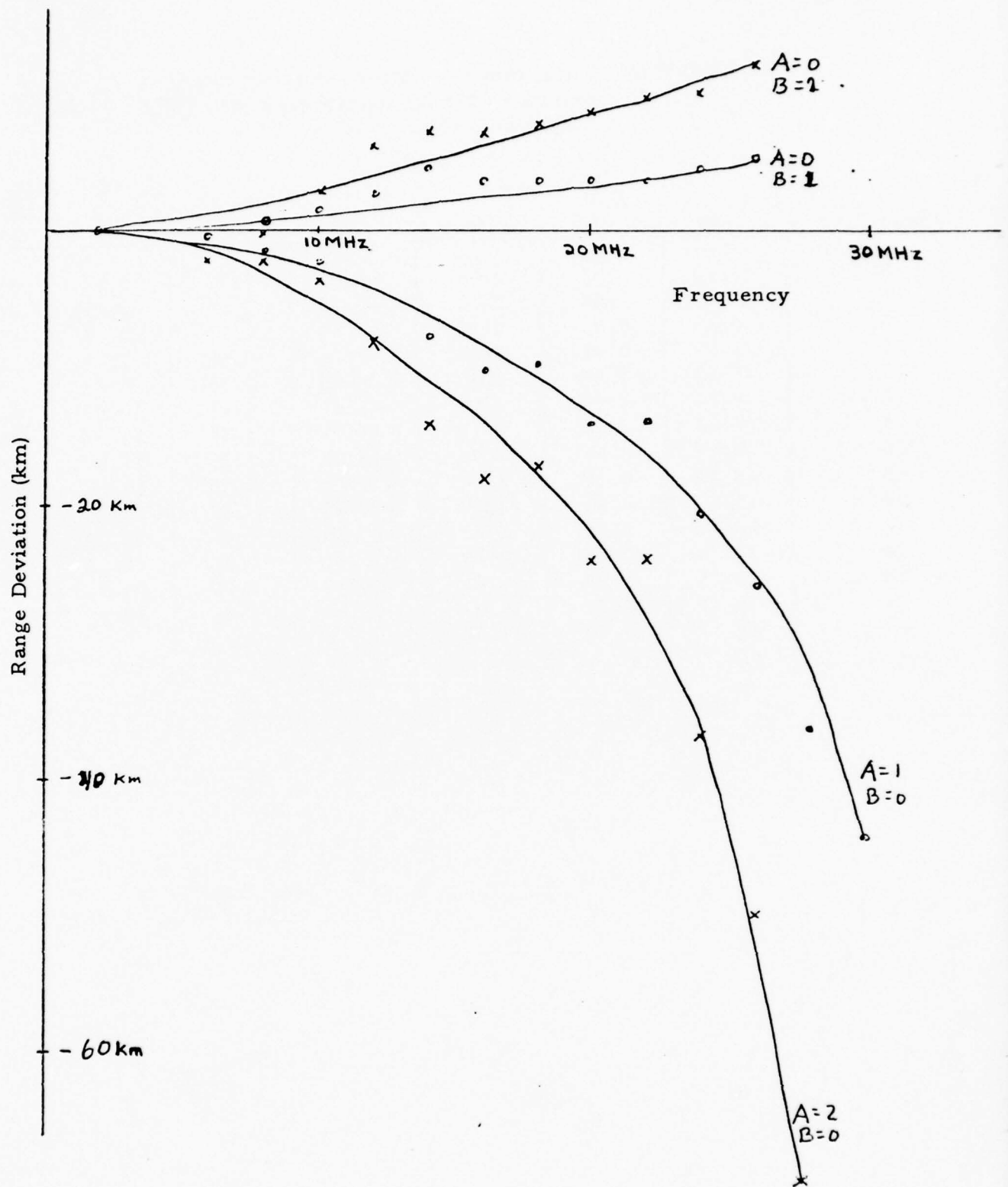


Fig. 8. Frequency Dispersion in Range Deviation Fitting Parameter.

Range Deviation

+120km

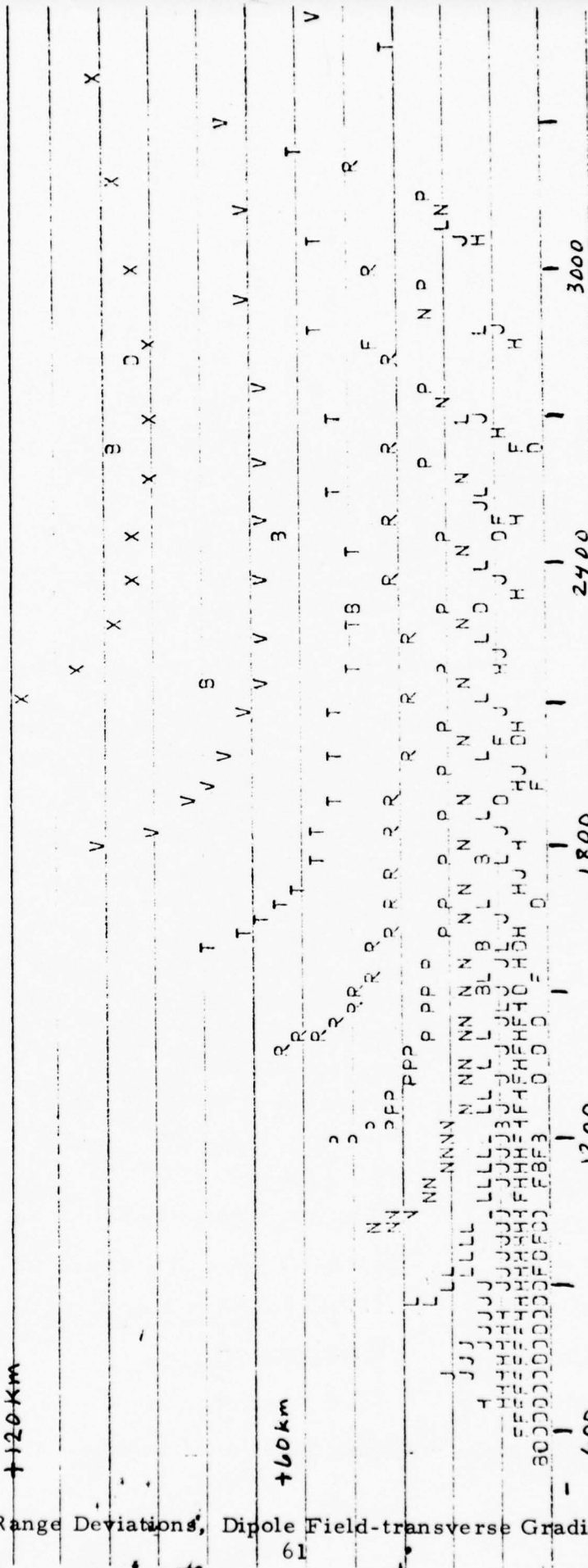


Fig. 9. Range Deviations, Dipole Field-transverse Gradient (B=1).

Range Deviation

+120 Km

+60 Km

600

1200

1800

2400

3000

Range (km)

Fig. 10. Range Deviations, Dipole Field-transverse Gradient (B=2).

BEST AVAILABLE COPY

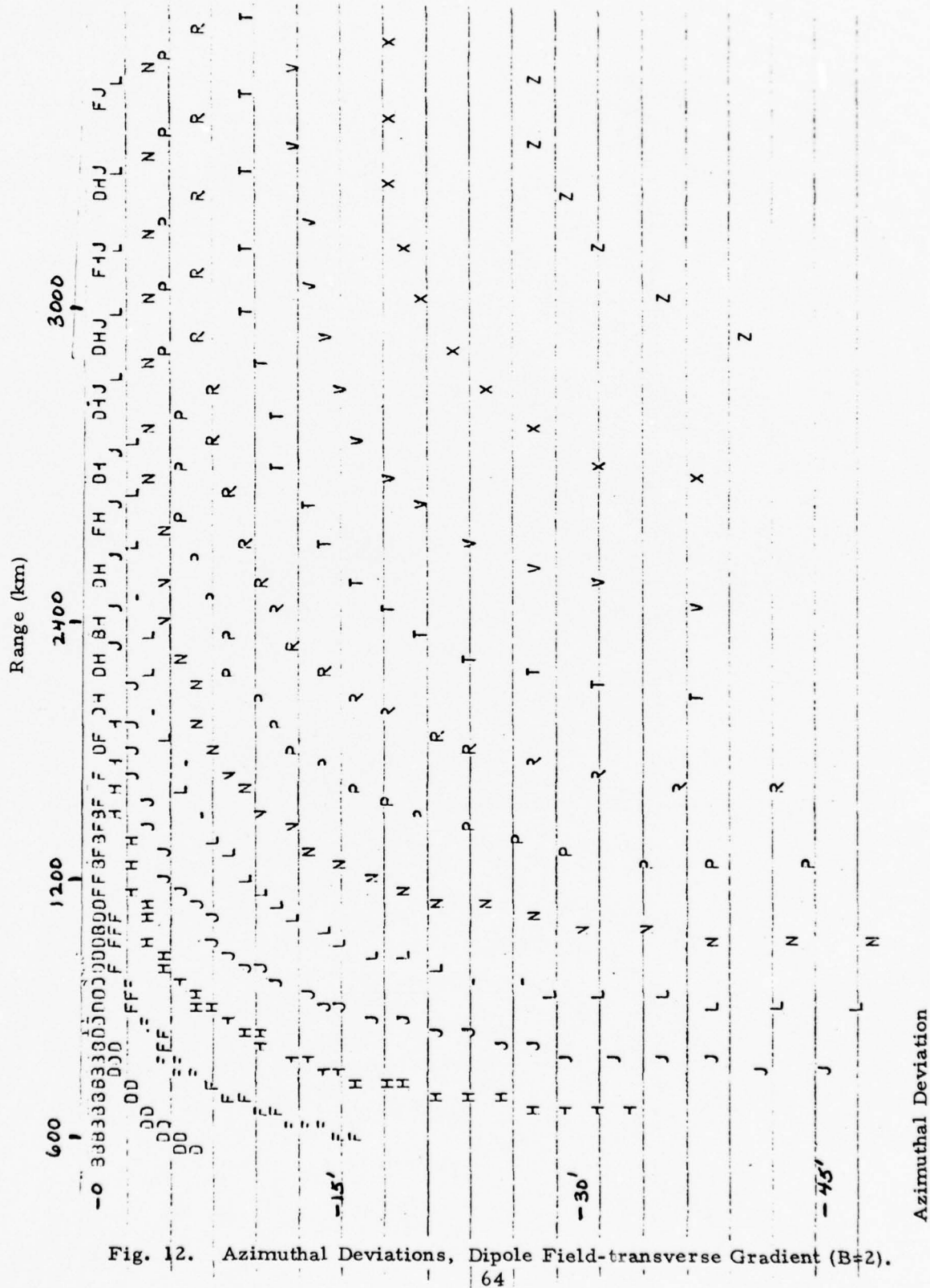


Fig. 12. Azimuthal Deviations, Dipole Field-transverse Gradient (B±2).

extremely sensitive to small changes in elevations near the minimum group path length. Furthermore, frequency dispersion of the transverse effects is well defined.

Figures 13 and 14 present azimuthal deviations as functions of takeoff elevation.

Several interesting features of the effects of gradients in critical frequency are worthy of notice. In the first place, effects due to the magnetic field are small and important primarily at lower frequencies. This, of course, was expected since the gyrofrequency is of the order of 1 megahertz. Secondly, the effects exhibit a well separated frequency dispersion. Thirdly, the effects appear to be fundamentally proportional to the magnitude of the appropriate derivative of critical frequency.

It does not appear likely that these features are to be simply related to parameters of the total path such as total group path length and ground to ground range. These quantities include considerable free space propagation, more or less depending on takeoff elevation. The important contribution for this study is, of course, from the integration through the ionosphere.

A productive method of fast and accurate ray tracing is to use a simple electron density model, such as the quasiparabolic model, which has an analytic solution to the ray trace equations, and allow this ionosphere to be tilted; i. e., the center of curvature of the spherically symmetric ionosphere is displaced from the center of the earth. Such a "tilted" ionosphere is then described by the layer parameters, and additionally by parameters specifying the center of curvature and lift of the model ionosphere. Clearly, the latter quantities will depend on the gradients of the ionospheric parameters, and also on the frequency and elevation of each ray.

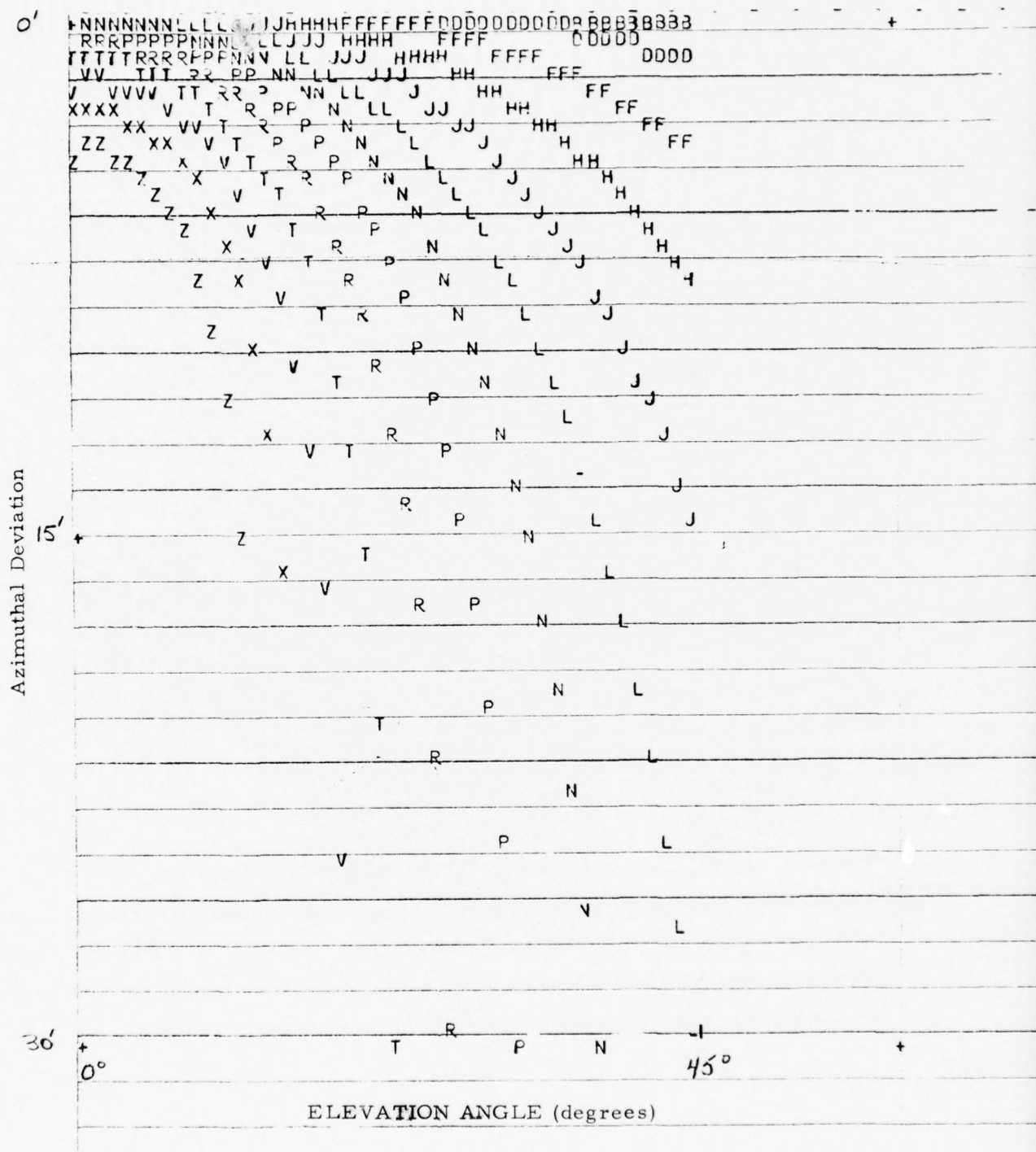


Fig. 14. Azimuthal Deviations vs. Elevation (B=1).

Consider the sets of ray traces through the ionospheres with longitudinal gradients in critical frequency ($A = 1$ and 2). Because of this gradient, a ray entering the ionosphere at a local elevation angle γ will exit the ionosphere at a local elevation angle $\gamma' \neq \gamma$. The effective tilt of the ionosphere for this ray, then, is given by $(\gamma' - \gamma)/2$.

Inspection of a small sample of these ray traces revealed that the effective tilt is strongly correlated with the penetration depth Δ_P of the ray into the ionosphere. This correlation for all rays is displayed in Figure 15. The x axis is the penetration depth, the y axis is the "normalized effective tilt," NET given by

$$\text{NET} = (\gamma' - \gamma)/2A$$

Plotted points "1" are rays from the set $A = 1$, "2" are rays from the set $A = 2$, and "*" are points resulting from a least square fit of the NET's given by

$$\text{NET}^* = a x + b x^2$$

where $x = \Delta_P/y_m$, $a = 1.04$ and $b = 1.37$; the standard deviation of the fit for all rays with penetration depth exceeding 10 kilometers ($x = 0.1$) is 0.11. This fit is good for small x but fails to adequately model the high angle rays. However, the most important feature of this correlation is that the frequency dependence is nearly completely contained in the penetration depth.

A significant improvement in analyzing NET can be effected by choosing the virtual height h_v of the equivalent ray (see Figure 3) in lieu of penetration depth as the independent variable. The resulting correlation is shown in Figure 16. The plotted points appear to be levelling off for the high angle rays; three terms may be desired to improve the fit. The fitting function plotted is given by

$$NET^* = a x + b x^3$$

where $x = (h_v - h_b)/y_m$. Other functions considered to model NET were $a x$, and $a x + b x^2$. The fitting parameters and standard deviations σ of these three fitting functions are listed in Table IV.

TABLE IV: Fitting Parameters for NET

<u>Function</u>	<u>a</u>	<u>b</u>	<u>σ</u>
NET ¹ = ax	.606	-	.039
NET ² = ax + bx ²	.577	.045	.027
NET* = ax + bx ³	.598	.010	.033

CONCLUSIONS:

We have found that the effective tilt of a parabolic ionosphere with longitudinal gradients allowed in the critical frequency can be well represented by a function of the form

$$T(f, \gamma_v) = \frac{1}{f_c} \frac{\partial f_c}{\partial \Theta} (a x + b x^2) \quad (33a)$$

where

$$T = (\gamma' - \gamma)/2$$

$$x = (h_v - h_b)/y_m$$

$$a = 0.577 \text{ degrees} = 0.01007 \text{ radians}$$

$$b = 0.045 \text{ degrees} = 0.00079 \text{ radians}$$

Angles γ' and γ are the local elevations of the ray at exit and entry respectively to the ionosphere at the base level altitude h_b , γ_v is the elevation angle of the virtual ray at the virtual height h_v , f is the operating frequency, f_c is the critical frequency of the layer, and y_m the semithickness.

The displacement D of the center of curvature of the equivalent ionosphere is given by

$$D = (r_o + h_v) \tan T \approx (r_o + h_v) T \quad (33b)$$

This result leads us to advance the following conjecture as a basis for formulating a fast ray tracing algorithm in ionospheres with gradients in the critical frequency. The presence of gradients in the critical frequency of the reflecting ionospheric layer may be accounted for by assuming an effective tilted spherical ionosphere the center of curvature of which is displaced from the center of the earth by the vector

$$\overline{D}_f = -r_v F(x) \overline{\text{grad } f_c / f_c} \quad (34)$$

where

$$F(x) \approx 0.01007 x + 0.00079 x^2 \quad (35)$$

and the gradient is to be evaluated at the virtual reflection point.

If, on the other hand, the critical frequency and semithickness did not vary but gradients existed in layer height h_m then the ionosphere is patently tilted with the center of curvature given by

$$\overline{D}_h = r_v \overline{\text{grad } h_m} \quad (36)$$

Furthermore, gradients in semithickness alone could presumably be reduced to an equivalent displacement of the center of curvature

$$\overline{D}_y = r_v Y(x) \overline{\text{grad } y_m} \quad (37)$$

In addition, the equivalent ionosphere could be lifted under the influence of gradients in the parameters either separately or because of coupling. This "lift" may be expressed as

$$\overline{D}_l = \overline{r}_v L(x, \{v\}) \quad (38)$$

where the argument set $\{v\}$ includes the ionospheric parameters and their gradients.

No conjectures are being advanced at present for the form of the functions Y and L .

A possibly useful conjecture to consider for the general case is that the center of curvature of the equivalent ionosphere is given by

$$\overline{D} = \overline{D}_f + \overline{D}_h + \overline{D}_y + \overline{D}_l \quad (39)$$

REFERENCES

1. Haselgrove, J., "Ray Theory and a New Method for Ray Tracing," *Prc. Camb. Conf. Phys. Ionosphere* (The Physical Society, London 1954).
2. Jones, R. M., "A Three-Dimensional Ray Tracing Computer Program," ESSA Tech Report IER-17/ITSA-17 (1966).
3. Croft, T. A. and Hoogasian, H., "Exact Ray Calculations in a Quasi Parabolic Ionosphere with no magnetic field," *Radio Science* 3, 69. (January 1968).
4. Barghausen, A. F., et al, "Predicting Long-Term Operational Parameters of High-Frequency Sky-Wave Telecommunication Systems," ESSA Technical Report ERL-110/ITS-78, U.S. Government Printing Office (Washington, 1969).
5. Westover, D. E., "Exact Ray-Path Solutions in a Quasi Linear Ionosphere," *Radio Science* 3, 75 (January 1968).
6. Folkestad, K., "Exact Ray Computations in a Tilted Ionosphere with no magnetic field," *Radio Science* 3, 81 (January 1968).
7. R. I. Beckwith, A. D. Bailey and N. N. Rao, "An Investigation of Directional Propagation Effects in High-Frequency Radio Source Location," RRL Publication No. 409, September 1972, Radiolocation Research Laboratory, Department of Electrical Engineering, University of Illinois, Urbana, Illinois 61801.
8. R. I. Beckwith, "A Computer Program for the Rapid Prediction of Angles of Arrival of HF Radio Waves," RRL Publication No. 442, November 1973, Radiolocation Research Laboratory, Department of Electrical Engineering, University of Illinois, Urbana, Illinois, 61801.
9. IAGA Commission 2, Working Group 4, "IGRF 1965.0," *Journal of Geophysical Research* 74, No. 17, 4407-4408, (1969).
10. Gilbert D. Mead, "IGRF 1965.0 in Dipole Coordinates," *Journal of Geophysical Research* 75, No. 22, 4372-4374, (1970).
11. Rao, N. N., "Inversion of Sweep-frequency Sky-wave Backscatter Leading edge for Quasiparabolic Layer Parameters," *Radio Science* 9, 845 (1974).

III. VERTICAL ELECTRON DENSITY MODELS IN THE POLAR REGION

In Section I, we have described improvements made to the ITS monthly median model for foF2 which allow for a more accurate description of the morphological features of the polar ionosphere. In earlier work,⁽¹⁾ we have described models applicable in the polar region for some other ionospheric parameters such as, foE, foF1, $h_m E$, $h_m E$, $h_m F1$ and $h_m F2$. These parameters were combined with several empirical models to produce a three-dimensional electron density distribution which could be used in various applications. In one application, electron density distributions are obtained on a uniform spherical grid for use with the ARCON Version II three dimensional ray tracing program. A grid is chosen such that the transmitter is at the north pole of the coordinate system. This coordinate system minimizes the amount of data needed to carry out any ray tracing study.

Extensive studies with this model have shown some areas in which the ionosphere is not correctly represented. We will describe here a new formulation for a vertical electron density distribution when one has estimates for the various ionospheric parameters which describe some of the individual layers. One area in which an improvement was sought was in the E region when increased ionospheric activity resulted in an elevated value of foE such that the probability of there not being a monotonic vertical electron density distribution was large.

Since the ionospheric parameters for the various layers have been determined independently of each other, the vertical electron density distributions must be constructed in a manner which is internally consistent and which does not contain any spurious horizontal gradients.

An example of an inconsistency would be a prediction of the height for an F1 layer at a higher altitude than that for the maximum density of the F2 layer. In general, the parameters are functions of the geographic and geomagnetic spatial coordinates, universal time, sunspot number and magnetic activity. The following Table lists the parameters used in the generation of a profile.

<u>Parameter</u>	<u>Needed for Profile</u>	<u>Model Used</u>
foF2	Required	ITS plus modifications (Section I)
$h_m F2$	Required	Reference 1
$y_m F2$	Required	Reference 1
foF1	Optional	Reference 1
$h_m F1$	Optional	Reference 1
foE _s (Solar)	Optional	Reference 1
foE _A (Auroral), $h_m E_A$	Optional	Reference 1 with modifications
$h_m E_s, y_m E$	Optional	Reference 1

The parameters for the F1 and E region are in general functions of local time (solar zenith angle) and may, therefore, be present only in certain geographical regions. We have attempted to allow for a smooth variation of the profile as one or more of these layers appears or disappears from the ionosphere. For a given set of conditions, all the desired parameters are first obtained separately. When both the solar E and auroral E layers are present, these parameters are combined to produce parameters that describe a single E layer. These two parameters, foE and $h_m E$ are generated according to the rules.

$$(foE)^4 = (foE_s)^4 + \frac{3}{2} (foE_A)^4$$

$$h_m^E = \frac{(foE_s)^2 h_m^E_s + (foE_A)^2 h_m^E_A}{(foE_s)^2 + (foE_A)^2}$$

The electron density $N(h)$ above the maximum height of the F2 layer is given in terms of two profiles. Between h_m^{F2} and a height Z_c , $N(h)$ is defined by a Chapman layer,

$$N(h) = N_m^{F2} \exp[1 - \xi - \exp(-\xi)]$$

where ξ is a scale height,

$$\xi \equiv \frac{h - h_m^{F2}}{y_m^{F2}} \quad \text{and}$$

$$N_m^{F2} = 1.24 \times 10^4 (foF2)^2 \quad \text{el/cc.}$$

The altitude $Z_c = Z_t + h_m^{F2}$ the low end of the topside profile is obtained as the solution of the cubic equation:

$$Z_t^3 + \frac{\zeta\beta}{4} Z_t^2 + \gamma Z_t - \frac{\zeta\beta}{4} y_\beta^2 = 0 \quad \text{where}$$

the coefficients are

$$\beta = \frac{1}{a\zeta}$$

$$\gamma = \beta^2$$

$$y_B = 1.25 y_m F2$$

and $a = 3.14 \times 10^{-4}$

$$\begin{aligned} \zeta = & 5.88 - 0.15 \lambda_m \cos \chi \\ & + 0.41 \cos \left\{ \frac{2\pi}{365} (D + 11) \right\} \sin \lambda - 0.14 K_p \end{aligned}$$

where $\lambda_m =$ corrected geomagnetic latitude

$\lambda =$ geographic latitude

$\chi =$ solar zenith angle

$D =$ Day number (1-365)

For $h \geq Z_c$ the topside profile is

$$N(h) = N_o \exp \left\{ -\zeta \left[\tan^{-1}(a\zeta h) - \tan^{-1}(a\zeta Z_c) \right] \right\}$$

where $N_o = N(h = Z_t + h_m F2)$ as determined from the Chapman layer.

Below $h_m F2$, there are four possible profiles depending upon which layers are present and the values of the layer parameters relative to each other.

If no E layer is present, it is also assumed that no F1 layer exists. In this case, we use as our profile model a single cubic function for the electron density using the three parameters f_oF2 , $h_m F2$ and $y_m F2$. The thickness of the layer is defined as

$$y_A = \sqrt{2} y_m F2 .$$

The electron density as then given by

$$N(h) = N_m F2 \left\{ 1 + 2 \left(\frac{h_m F2 - h}{y_A} \right)^3 - 3 \left(\frac{h_m F2 - h}{y_A} \right)^2 \right\}$$

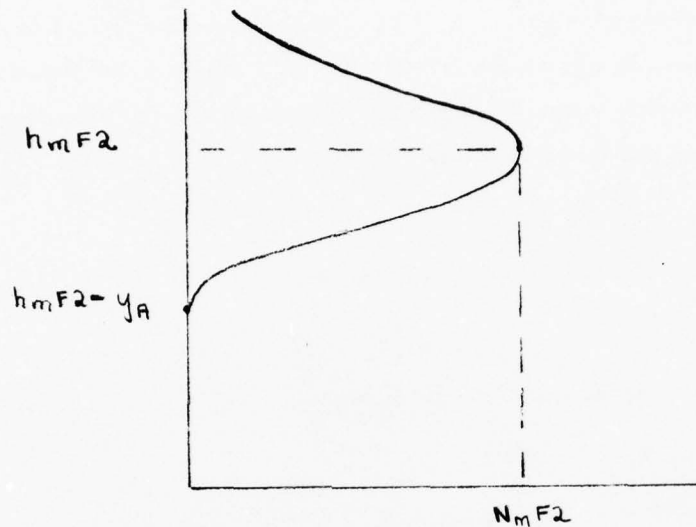
Using this profile, the height $h_m = h_m F2 - 1.3 y_m F2$ is such that

$$N(h_m) = 0.01 N_m F2$$

We require that the model not produce a density greater than this value below a specified height h_{min} (taken at this time to be 140 km.) If $h_m < h_{min}$, we redefine the thickness of the layer such that $N(h_{min}) = 0.01 N_m F2$ by the following shrinkage of the layer:

$$y_A = \frac{1.3}{\sqrt{2}} (h_m F2 - h_{min}) .$$

The following is a sketch of a sample profile showing the relevant parameters.



In the event that an E layer exists but that there is no F1 layer, the profile falls into two categories. In the first case, the electron density is a monotonic function of altitude. In the second case, the electron density decreases to a minimum value between the heights of the E layer and F2 layer maximum densities. The choice of which profile is used is based upon the following criteria.

For a monotonic profile to be used, we require that the electron density distribution in the F2 region not fall too rapidly so as to be inconsistent with the electron density at the E layer maximum. One possible statement of this condition is that

$$h_m E \geq h_m F2 - \sqrt{2} y_m F2 \quad (A)$$

If this test is satisfied, we then calculate the frequency f_E at $h_m E$ from a cubic F2 layer profile using the following expression:

$$f_E^2 = (f_o F2)^2 \left\{ 1 + 2 \left(\frac{h_m F2 - h_m E}{y_A} \right)^3 - 3 \left(\frac{h_m F2 - h_m E}{y_A} \right)^2 \right\} .$$

The second condition for a monotonic profile is that f_E as predicted from a F2 layer by greater than $f_o E$ the value determined from an independent model for the E region.

$$f_E(h_m E) \geq f_o E(h_m E) \quad (B)$$

When this condition is not met, the F2 region electron density has dropped too rapidly to be consistent with an independent by predicted density for the E region.

The monotonic profile used is of the following form:

$$(i) \text{ F2 region} \quad h_m E \leq h \leq h_m F2$$

$$N(h) = N_m F2 + (N_m F2 - N_m E) \left\{ 2 \left(\frac{h_m F2 - h}{h_m F2 - h_m E} \right)^3 - \left(\frac{h_m F2 - h}{h_m F2 - h_m E} \right)^2 \right\}$$

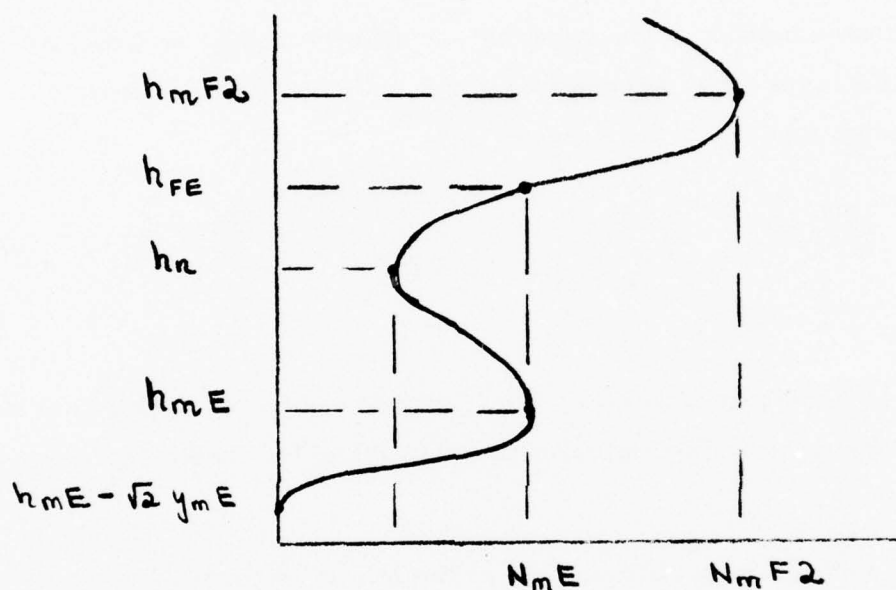
$$(ii) \text{ E region} \quad h_m E - \sqrt{2} y_m E \leq h < h_m E$$

$$N(h) = N_m E \left\{ 1 + 2 \left(\frac{h_m E - h}{\sqrt{2} y_m E} \right)^3 - 3 \left(\frac{h_m E - h}{\sqrt{2} y_m E} \right)^2 \right\}$$

$$(iii) N(h) = 0 \quad h < h_m E - \sqrt{2} y_m E$$

This profile is also used in the event that $foE \geq foF2$.

When either condition A) or B) is not satisfied, a profile of the type shown in the following figure is used.



A parabolic layer is used in the F2 region. This profile is used to determine the height, h_{FE} at which $N(h_{FE})$ in the F2 region is equal to $N_m E$. A cubic equation is then used in the region between this height and $h_m E$ which maintains both a continuous electron density and its height derivative. If we take

$$N(x) = ax^3 + bx^2 + cx + d \quad \text{where} \quad x = h - h_m E$$

then we require the following conditions for the coefficients

$$(a) \quad N(o) = N_m E = d$$

$$(b) \quad \frac{\partial N}{\partial x} (o) = o = c$$

$$(c) \quad N(h_{FE} - h_E) = N_m E$$

$$(d) \quad \frac{\partial N}{\partial x} (h_{FE} - h_E) = \frac{\partial N}{\partial h} (h_{FE}, \text{ F2 layer})$$

These conditions determine a cubic which has a minimum at the height

$$h_n = h_m E + \frac{2}{3} (h_{FE} - h_m E)$$

The complete profile is then:

$$(i) \quad \text{F2 region} \quad h_{FE} \leq h \leq h_m F2$$

$$N(h) = N_m F2 \left\{ 1 - \left(\frac{h_m F2 - h}{\sqrt{2} y_m F2} \right)^2 \right\}$$

$$(ii) \quad h_m E \leq h < h_{FE}$$

$$N(h) = N_m E + \frac{A(h - h_m E)^2}{(h_{FE} - h_m E)} \left\{ \left(\frac{h - h_m E}{h_{FE} - h_m E} \right) - 1 \right\}$$

where $h_{FE} = h_m F2 - \sqrt{2} y_m F2 \left\{ 1 - \left(\frac{foE}{foF2} \right)^2 \right\}^{1/2}$

and $A \equiv \frac{\partial N}{\partial h}(h_{FE}) = \frac{2 N_m F2}{\sqrt{2} y_m F2} \left\{ 1 - \left(\frac{foE}{foF2} \right)^2 \right\}^{1/2}$

(iii) E region $h_m E - \sqrt{2} y_m E \leq h < h_m E$

$$N(h) = N_m E \left\{ 1 + 2 \left(\frac{h_m E - h}{\sqrt{2} y_m E} \right)^3 - 3 \left(\frac{h_m E - h}{\sqrt{2} y_m E} \right)^2 \right\}$$

The electron density in region (ii) at h_n is

$$N(h_n) = N_m E - \frac{8}{27} N_m F2 \left(\frac{h_{FE} - h_m E}{\sqrt{2} y_m F2} \right) G$$

where $G \equiv \left\{ 1 - \left(\frac{foE}{foF2} \right)^2 \right\}^{1/2}$

We made the additional requirement that the minimum density, $N(h_n)$ $N(h_n) \geq \frac{1}{9} N_m E$. If this is not the case, we set $N(h_n) = \frac{1}{9} N_m E$ and use the profile in this region to redefine the semithickness of the F2 region obtaining

$$y_m^{F2} = \frac{1}{\sqrt{2}} \left\{ \frac{N_m^{F2} \cdot G \cdot (h_m^{F2} - h_m^E)}{3 N_m^E + G^2 N_m^{F2}} \right\}$$

The final case is when all three layers, F2, F1 and E are to be present. Here, we also require that the electron density within each layer be consistent with that predicted independently for the contiguous layer. The thickness of each layer is defined:

$$y_c = h_m^{F2} - h_m^{F1}$$

and

$$y_D = h_m^{F1} - h_m^E$$

A three layer profile is used when $y_c \geq y_m^{F2}$. If this condition is not satisfied, we assume that the electron density in the F2 region cannot fall fast enough to account for the existence of an F1 layer at its predicted position. When this occurs and $foF1 \geq foE$, we neglect the F1 layer and use a two layer monotonic profile as was previously described. If $foF1 < foE$, we still omit the F1 layer but use the nonmonotonic profile of an E and F2 layer.

The three layer profile consists of the following:

$$(i) \text{ F2 region} \quad h_m^{F1} \leq h \leq h_m^{F2}$$

$$N(h) = N_m^{F2} + (N_m^{F2} - N_m^{F1}) \left\{ 2 \left(\frac{h_m^{F2} - h}{y_c} \right)^3 - 3 \left(\frac{h_m^{F2} - h}{y_c} \right)^2 \right\}$$

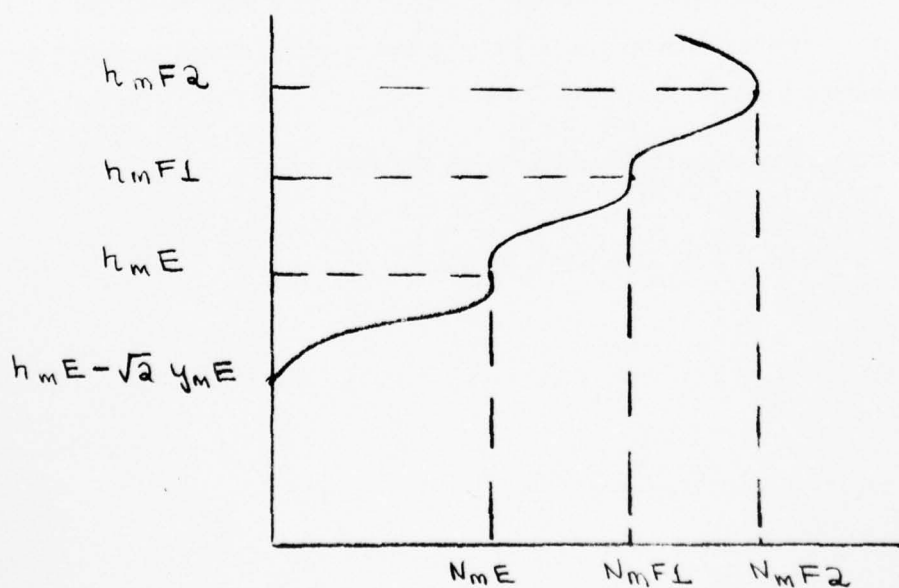
(ii) F1 region $h_m^E \leq h < h_m^{F1}$

$$N(h) = N_m^{F1} + (N_m^{F1} - N_m^E) \left\{ 2 \left(\frac{h_m^{F1} - h}{y_D} \right)^3 - 3 \left(\frac{h_m^{F1} - h}{y_D} \right)^2 \right\}$$

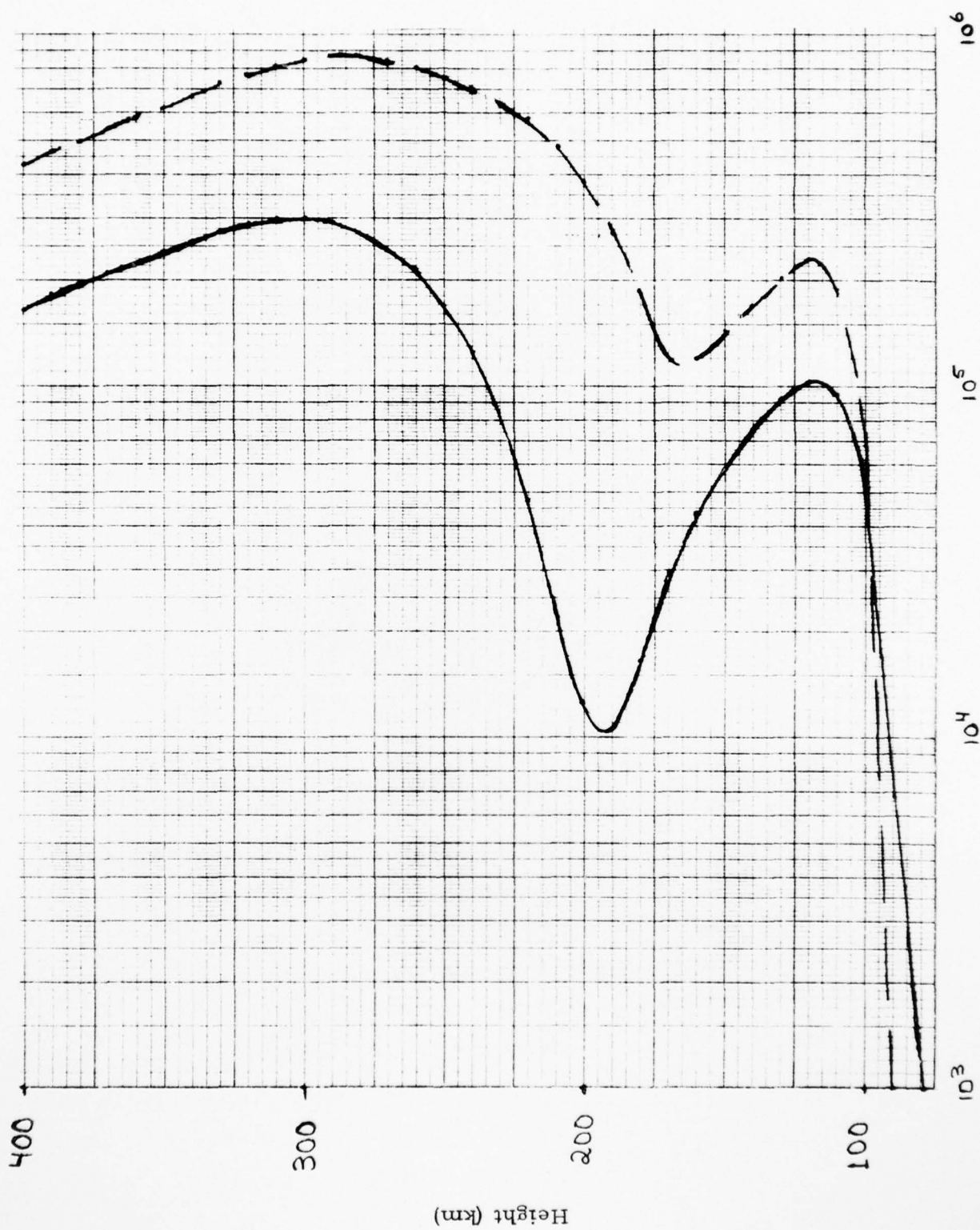
(iii) E region $h_m^E - \sqrt{2} y_m^E \leq h < h_m^E$

$$N(h) = N_m^E \left\{ 1 + 2 \left(\frac{h_m^E - h}{\sqrt{2} y_m^E} \right)^3 - 3 \left(\frac{h_m^E - h}{\sqrt{2} y_m^E} \right)^2 \right\}$$

These are three cubic profiles with $\frac{\partial N}{\partial h} = 0$ at each layer height of maximum electron density. No other conditions are placed upon the layer parameters other than those already stated so that the profile need not be monotonic. It is possible that the maximum electron density occur at either the F1 or E layer maximum height. A sample profile is shown below.



VERTICAL ELECTRON DENSITY PROFILES



Electron Density (el./cc.)

Figure III-1

Figure III-1 illustrates two vertical electron density distributions for the case in which $f_oF1=0$. The parameters used in the calculation of the electron density at 10 km intervals are the following:

<u>Parameter</u>	<u>Solid Curve</u>	<u>Dashed Curve</u>
Local Time	16.7	13.3
Latitude	26.9°	31.3°
Longitude	341.2°	289.1°
Sec χ	-5.87	6.42
$f_o E$	3.0 MHz	4.65 MHz
$f_o F2$	5.2	8.7
$y_m F2$	47.6 km	85.4 km
$h_m E$	113.6	117.9
$h_m F2$	312.7	289.0
h_{min}	194.0	163.9

The value $N(h_{min})$ for the solid curve is constrained to be $1/9 N_m E$.

In many applications, the vertical electron density model is used to generate a three-dimensional electron density distribution in space and time. This requires that the longitudinal gradients generated by using the model at different points in space be consistent with those that are observed. Since we may use an entirely different profile depending upon the values of ionospheric parameters, care must be used in specifying the closeness of the calculated profiles. Examples of two

dimensional ionospheres is shown in Figures III-2 and III-3 where contours of constant electron density are shown as a function of height above the earth and angular range for a great circle path of 50° . In both figures, the electron density is calculated at height intervals of 10 km using our vertical electron density distributions. In Figure III-2, the profiles are calculated at angular intervals of 5° whereas in Figure III-3 the interval is 1° . The isoionic contours are then drawn using a quadratic smoothing technique using the respective grids of (11, 33) and (51, 33) data points.

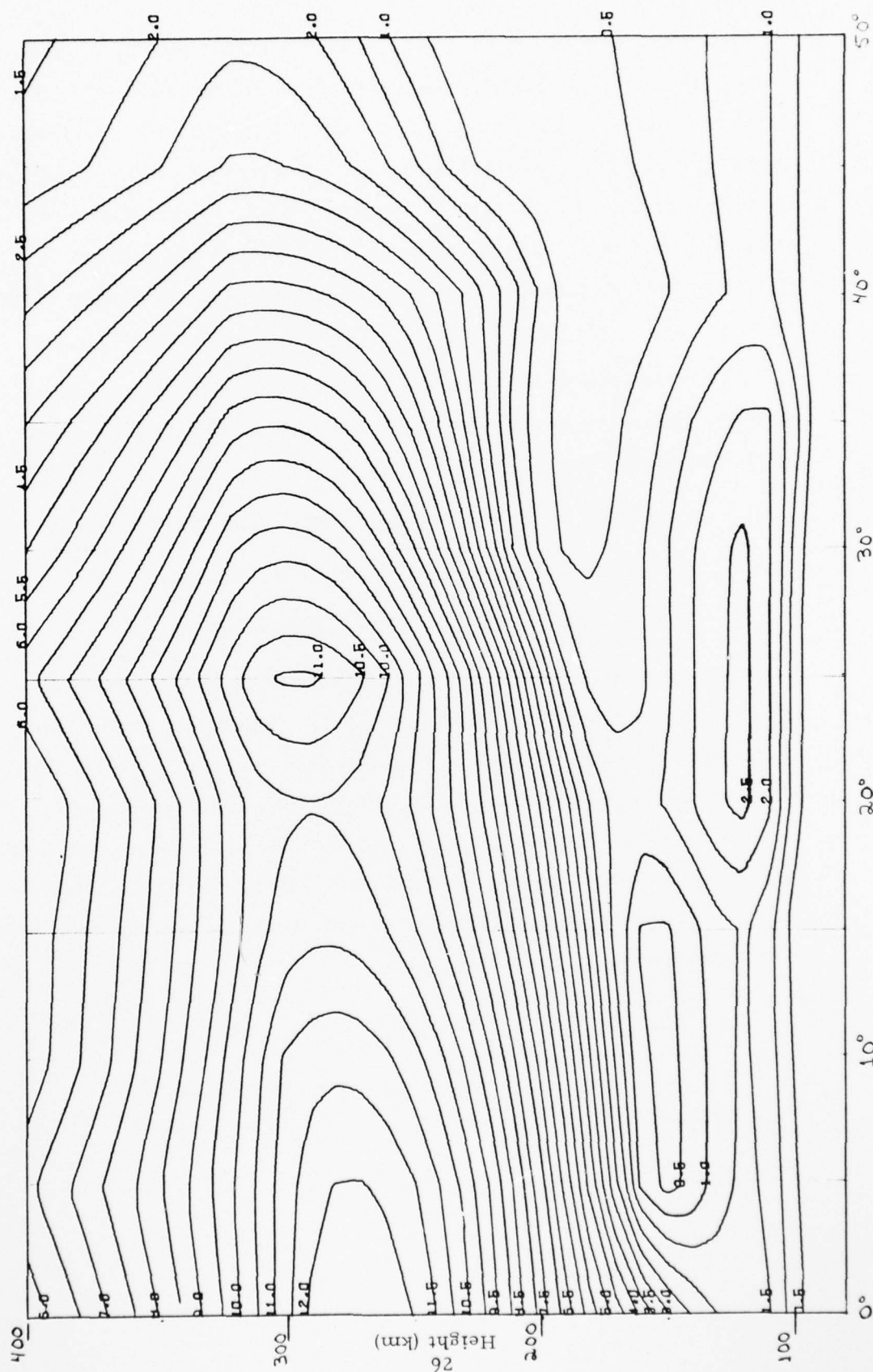
Although most of the features contained in each of the figures are similar, there are some regions in which large differences exist. The most notable of these are:

- a) Lower E region, $\theta = 4^\circ$, height = 150 km.
- b) Lower E region, $\theta = 18^\circ$, height = 125 km.
- c) Lower F region, $\theta = 38^\circ$, height = 200 km.

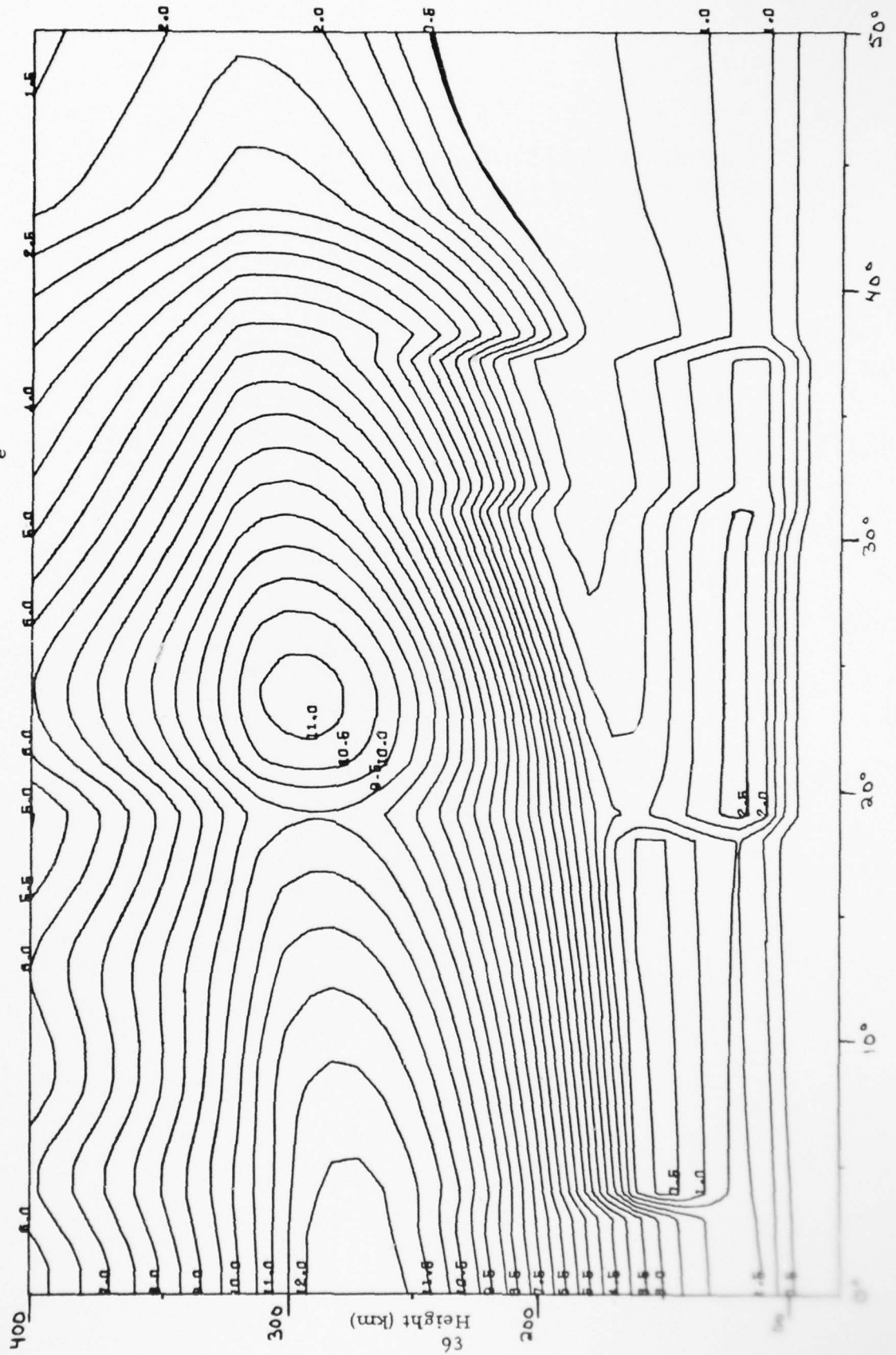
The gradients in each of these regions for the ionosphere of Figure III-3 is a factor five times that of Figure III-2. This is due to the interpolation of contours of constant electron density from vertical profiles which are specified at intervals that are five times more closely spaced. If the interval were more closely spaced, these gradients would become even larger. This deficiency in the model can be surmounted by matching the fineness of the choice of the grid spacing with the magnitude of the gradients of electron density occurring in the ionosphere.

BEST AVAILABLE COPY

CONTOURS OF CONSTANT ELECTRON DENSITY ($N_e \cdot 10^{-5}$ el./cc.)



Great Circle Range (Degrees)
Figure III-2



Great Circle Range (Degrees)

AD-A038 298

ARCON CORP WAKEFIELD MASS
IONOSPHERIC ANALYSIS AND IONOSPHERIC MODELING.(U)
FEB 77 D C MILLER, J GIBBS

F/G 20/14

UNCLASSIFIED

RADC-TR-77-53

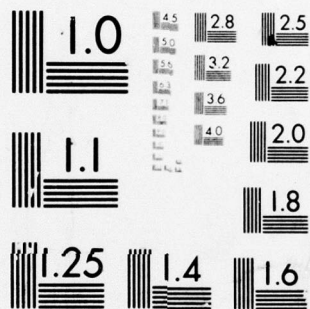
F19628-74-C-0070
NL

2 OF 2
AD
A038 298



END

DATE
FILMED
5-77



MICROCOPY RESOLUTION TEST CHART
NATIONAL BUREAU OF STANDARDS-1963-A

REFERENCES

1. Miller, D. C. and Gibbs, J. (1975) Ionospheric Analysis and Ionospheric Modeling. AFCRL-TR-75-0549.
2. Miller, D. C. and Gibbs, J. (1974) Ionospheric Analysis and Ionospheric Modeling. AFCRL-TR-74-0364.

IV. COORDINATE CONVERSION TECHNIQUE FOR OTH BACKSCATTER RADAR

Detailed documentation of the program WIMP and its ionospheric and mathematical techniques has been prepared for the Electromagnetic Sciences Division of the Deputy for Electronic Technology. This writeup along with an annotated program listing is contained in a separate report.

The WIMP Program is a complex algorithm which performs an accurate conversion from radar target range coordinates to geographic target coordinates in OTH Backscatter HF radar applications. The complexity is due to the use of a iterative algorithm that involves interaction between the program and the user. The program consists of three main components:

- a. A set of subprograms which construct a three-dimensional three-layer ionospheric model.
- b. A set of subprograms which simulate HF radio wave propagation in the ionosphere constructed in (a).
- c. One of three driving programs controlling the calling sequence to the radio wave propagation simulator in (b). These driving programs perform the following tasks: (1) From a given ionosphere, generate the leading edge of a simulated oblique ionogram including scale factors to the F_2 layer parameters to force agreement with a given vertical ionogram; (2) from a comparison of the simulation in (1) to a given oblique ionogram generate range gradient factors to apply to $f_o F_2$ and $M(3000)F_2$ to force agreement; (3) from the final ionosphere generated in (1) and (2), simulate predicted radio frequency propagation paths, from which range versus group path functions may be tabulated.

The writeup contains a description of the WIMP three-dimensional three-layer ionospheric model, followed by a general description of the radio wave propagation simulation subprogram (ray-tracing algorithm). A functional description is given of the three driving programs and the operating instructions for their use are included.

Program block diagrams, flow charts, and program listings are included in appendixes.

Comparisons have been made of the results of the WIMP ray tracings to techniques developed at RADC. The description and results of these studies are reported in a separate annex to this report.

MISSION
of
Rome Air Development Center

RADC plans and conducts research, exploratory and advanced development programs in command, control, and communications (C³) activities, and in the C³ areas of information sciences and intelligence. The principal technical mission areas are communications, electromagnetic guidance and control, surveillance of ground and aerospace objects, intelligence data collection and handling, information system technology, ionospheric propagation, solid state sciences, microwave physics and electronic reliability, maintainability and compatibility.



**Printed by
United States Air Force
Hanscom AFB, Mass. 01731**